Experimental and analytical study of the high-strain-rate compressive behavior of SFRC

Mohammad Bakhshi, Isabel B. Valente, Honeyeh Ramezansefat, Joaquim A. O. Barros, Eduardo N. B. Pereira & Nuno R. M. Peixinho

Published online: 13 Apr 2023.

Submit your article to this journal

View related articles

View Crossmark data

Taylor & Francis
Taylor & Francis Group

Check for updates

ORIGINAL ARTICLE

Experimental and analytical study of the high-strain-rate compressive behavior of SFRC

Mohammad Bakhshi[a], Isabel B. Valente[a], Honeyeh Ramezansefat[a], Joaquim A. O. Barros[a], Eduardo N. B. Pereira[a], and Nuno R. M. Peixinho[b]

[a]Department of Civil Engineering, Faculty of Engineering, University of Minho, Azurem, Guimaraes, Portugal; [b]Department of Mechanical Engineering, Faculty of Engineering, University of Minho, Azurem, Guimaraes, Portugal

ABSTRACT

The compressive behavior of steel-fiber-reinforced-concrete (SFRC) is dependent on the loading rate. This research investigates, experimentally and analytically, the effect of loading rate on the compressive behavior of SFRC designed to be used in prefabricated urban protective furniture. For this purpose, cylinder SFRC specimens were subjected to modified instrumented-drop-weight-impact tests at four dropping heights and quasi-static tests with four different strain rates. The inertia force was analytically obtained and also experimentally measured. The results demonstrate that by increasing the strain rate, elastic modulus, compressive strength, and energy dissipation capacity have increased. Three different models were proposed for predicting each mechanical characteristic, one in the range of quasi-static and the others in the range of impact corresponding to the split Hopkinson pressure bar and drop-weight-impact tests. The experimental dynamic to static ratios obtained for SFRC properties were discussed and compared with those proposed by present study and from other researchers. Three proposed models significantly improve the prediction the dynamic increase factor values in terms of compressive strength, modulus of elasticity and toughness.

1. Introduction

Concrete has become the most used construction material in the industry [1]. However, its relatively low tensile strength and deformability up to cracking, and its brittle nature under impact loadings, require the use of reinforcements disposed appropriately. This is a laborious task with significant influence on the final cost of certain construction systems, mainly those with some geometric complexity, such is the case of some safety protection systems [2]. Relatively short fibers have been used, as an extra concrete mixture constituent, alternatively to conventional continuous reinforcements. The aim is mostly to control the crack width and increase the load and deformation capacity after crack initiation, by taking advantage of the fiber pullout resisting mechanism, resulting in a composite generally designated by fiber reinforced concrete (FRC) [3, 4]. The energy dissipated due to the fiber pullout and/or tensile rupture causes a significantly higher performance of FRC under high strain rate loading comparing to the normal concrete [5].

Several types of fibers have been used in FRC, but steel fibers are still the predominant, in the so-called steel fiber reinforced concrete (SFRC), whose structural potentialities are extensively documented based on research [6–8] and real applications [9, 10]. Many studies report that steel fibers can also significantly increase the impact resistance and

energy dissipation capacity of concrete elements [11, 12]. Therefore, SFRC has been considered a suitable material for construction systems potentially subjected to impact loads in service conditions, such as the case of bridge decks and industrial, airport and harbor pavements [13, 14], as well as those specifically designed for protective systems to resist impact or explosive loadings caused by human attacks and extreme events [15, 16].

Concrete exhibits different properties under dynamic and static loading. The strain rate sensitivity of the compressive behavior of plain concrete was investigated by Bischoff and Perry [17]. They used different test approaches to determine the dynamic properties of the tested materials. Most of the studies established on the evaluation of the dynamic characterizations of SFRC are on the basis of experiments, and different experimental approaches have been developed for studying the mechanical characteristics of SFRC under impact loading. Several researchers [11, 18–24] have investigated the effect of strain rate on the mechanical behavior of FRC. Wang et al. [20] used the split Hopkinson pressure bar (SHPB) test to investigate the effect of strain rate on the compressive behavior of plain concrete and FRC with steel and polyethylene (PE) fibers. By executing SHPB tests at strain rates from about 10 to $300 \, s^{-1}$, they verified that by increasing the strain rate the SFRC's compressive strength

has enhanced. Moreover, by increasing the strain rate, the failure mode of the steel fibers in the SFRC has changed from pull-out to tensile rupture. Therefore, the maximum impact force has increased with the number of ruptured steel fibers, but the ductility of SFRC has decreased, due to the smaller energy absorption of tensile rupture over pull-out of the fibers. In another study, Wang et al. [21] carried out compressive tests on both SFRC and plain concrete specimens containing three different volume fractions (1.5%, 3% and 6%) of very short straight steel fibers. The results revealed that the compressive strength of SFRC increased with both the volume percent of steel fiber and the strain rate. Furthermore, the energy absorption in compression (compressive toughness, area under the obtained compressive stress-strain diagram) at higher strain rates has increased by using up to 3% of steel fibers volume fraction [21].

Lok and Zhao [19] and Lok et al. [18] used the SHPB test setup with a device's diameter of 75 mm to apply the compressive load at different high strain rates (from 20 to $110 \, s^{-1}$) in specimens made by hooked-end SFRC with 0.6% fiber volume fraction. The compressive strength of SFRC has considerably increased by increasing the strain rate, while the gradient of load decay in the post-peak force-deflection phase has increased with the strain rate. Accordingly, a maximum strain rate was suggested up to which this structural softening response is not detrimentally affected from the toughness behavior point of view. Hao and Hao [25] conducted an experimental study on the dynamic compressive behavior of spiral SFRC at different strain rates (from 50 to $200 \, s^{-1}$), by executing SHPB tests with a device's diameter of 75 mm. The results showed that the toughness of SFRC has increased with the volume fraction of fibers, due to the higher number of fibers controlling the cracking propagation process, decreasing the number and length of cracks and fragments.

Although there is no standard test recommended for determining the relevant properties of SFRC under compressive impact loading, instrumented drop weight tests have been used with standard SFRC cylinders for this purpose by Xu et al. [15]. In their experimental study, cold-rolled, hooked end, synthetic fibers, flattened, undulated, and two new spiral shape steel fibers were used. The study showed that FRC with new spiral fibers presents higher ultimate stress and energy-absorption capacity than other types of FRC specimens tested. They concluded that the shape of the fiber affects the mechanical properties and the strain rate sensitivity of FRC under compressive impact loading. The dynamic increase factor (DIF), which is the ratio between a material property evaluated in dynamic and static loading conditions, has been considered by many researchers as the main parameter for quantifying the influence of the strain rate on the compressive behavior of SFRC [12, 20, 21, 26–28]. Several models have been suggested for predicting the DIF for the concrete compressive strength [19, 21, 25, 26, 29, 30], but the one proposed by fib model code [30] is, maybe, the most used:

Reliable experimental data for assessing the predictive performance of existing models on the DIF of the relevant properties of SFRC in compression is still scarce. Therefore, the present research aims to investigate the effect of strain rate on the compressive behavior of SFRC with hooked end fibers by using standard specimens and the instrumented drop weight impact setup recommended by ACI Committee 544 [31]. Qualitative information, such as failure patterns and fracture surfaces, and quantitative data, such as compressive strength, strain at compressive strength, and energy absorption capacity are obtained for the evaluation of the compressive behavior of SFRC at the different loading rates. In addition, the inertial force during impact loading is also determined, due to its relevance for analytical modeling of the dynamic behavior of SFRC elements subjected to high strain rate loading conditions.

Based on the test results of SFRC specimens, the dynamic to static properties ratios of SFRC are discussed and compared with those recommended by CEB-FIP model code [30]. In addition, at different strain rates, the variation of the acceleration and the inertia force (as the main gap of knowledge in literature for SFRC under compressive impact loading) are analytically investigated and also experimentally measured at the mid-height of the curved outer surface of SFRC cylinders. The relation between strain rate, impact load, and inertia force is evaluated and discussed. Finally, in order to improve the prediction of DIF, some innovating empirical relationship is proposed for each mechanical characteristic considering the effect of test approach to explain the strain rate sensitivity of SFRC. Three different models are proposed for predicting each mechanical characteristic, one model in the range of quasi-static and two models in the range of impact correspond to the SHPB and drop weight impact tests.

2. Experimental program

2.1. Materials

Throughout the experimental program, one type of SFRC was studied, where the binder was composed by cement type-I (42.5 R) according to EN 197-1 (2011) with a specific density of 3.15 g/cm^3, and EN 450-1 (2012) type-II fly ash. The coarse and fine aggregates with maximum size of 12 mm (D_{max}) used were natural river sand and gravel, whose saturated surface dry densities were 2.64 and 2.60 g/cm^3, respectively. The aggregates were graded following BS-EN 933-1 (2012). The SIKA ViscoCrete 5920 superplasticizer was used. The mix design was calculated following the volume approach recommended by ACI-544-1R [6] for determining the proportion of the SFRC ingredients, Table 1. A volume fraction of 1% of the hooked-end steel fibers, whose geometric and mechanical properties are indicated in Table 2, was used. In the present study, it was assumed that the steel fibers in the mixture are uniformly distributed and randomly oriented.

Table 1. Mix proportions of SFRC per m^3.

Cement [kg]	Fly ash [kg]	Water-cement content ratio	Fine aggregate 0–4 mm [kg]	Coarse aggregate 4–12 mm [kg]	Superplasticizer [kg]	Steel fibers [kg]
400	200	0.3	942	628	4.8	78.5

Table 2. Characteristics of used steel fiber.

Volume [%]	Mass [kg/m^3]	Diameter (d_f) [mm]	Length (l_f) [mm]	l_f/d_f	Modulus of elasticity [GPa]	Tensile strength [MPa]
1	7850	0.38	30	80	210	2300

2.2. Test program

2.2.1. Quasi-static tests

Experimental tests were conducted according to EN 12390-3 recommendation to evaluate the compressive strength and modulus of elasticity of SFRC. Cylindrical specimens with 100 mm diameter and 200 mm height were chosen, so that the smaller dimension of the specimen is at least three times larger than l_f and D_{max} in order to avoid fiber orientation effect and aggregates segregation. Three specimens were tested for each strain rate level. The grinding method was used to smooth out the surface of hardened SFRC specimens. To perform the compressive tests under quasi-static loading, a servo hydraulic machine with load capacity of 3000 kN was adopted. Three linear variable differential transducers (LVDTs) were installed at the mid height of the specimen to measure the average compressive strain and modulus of elasticity under static loading (lowest loading rate of quasi-static tests). In quasi-static compressive tests, three strain gauges were used to measure the strain rate and compare it with the displacement rate measured with the LVDTs with length of 200 mm. The applied compressive force was measured by a load cell with capacity of 1000 kN installed on the loading machine. When the loading rate is increased, a higher recording rate (2–50 data per second), that is able to record the fast-response data, is selected in the data acquisition system.

The effect of strain rate on the compressive behavior of SFRC was investigated on cylindrical specimens. Relevant parameters, such as compressive strength, elastic modulus, and energy absorption capacity were measured for each loading rate. Figure 1 shows the position of the strain gauges (SG) on the specimens prepared for compression tests, as well as the test setup. As listed in Table 3, four different series of compression tests were carried out, which correspond to four different strain rates in the range of quasi-static loading. In this table, the distinctive designation of the specimens consists of two parts. The first part represents the type of the loading: "S" for the static loading, "Q" for quasi-static loading, and "HS" for high strain rate loading (impact). The following number for quasi-static and high strain rate loadings is the applied displacement rate and drop height of impactor, respectively. To determine the DIF of strain rate effect, all results obtained in the experiments conducted at different strain rates were related to the static strength measured at a specific quasi-static strain rate. For applying static load with the strain rate of 30×10^{-6} s^{-1} recommended by CEB-FIP model code [30] as a reference static strain rate, the displacement rate of 1 mm/min was applied. The maximum displacement rate possible to be applied by the adopted equipment was 500 mm/min, which matches a strain rate of 5.6×10^{-2} s^{-1}.

2.2.2. Instrumented drop weight impact test

An instrumented drop-weight setup was used for applying compressive impact loads which has the capacity to drop different masses from different heights, shown in Figure 2a. It can drop a maximum mass of 292 kg from a height of 9.1 m, corresponding to a theoretical contact velocity of 13.36 m/s. To ensure uniform load application throughout the entire cylinder's surface, in addition to smoothing the surface of each cylindrical SFRC using the grinding machine, its position was thoroughly verified both before and during testing using a high-speed video camera. The impact forces on bottom (reaction force) and top (impact force) of the specimens were recorded by two load cells with capacity of 2000 and 1000 kN, respectively. The inertia force may be calculated from the difference between the measures in these load cells, which were recorded by a data acquisition system connected to a PC. As multiple channels are utilized at the same time, this control card has a recording rate capacity of 50,000 data per second. A high-speed video camera was used to measure the deformation and failure process of specimens. The deformation measurements in the specimens during the impact loading process were used for calculation of strain and strain rates values. Three strain gauges at the mid-height of cylinders were also installed to directly measure strain and strain rates values, Figure 2a. In addition, two accelerometers were installed on the external surface of a cylinder specimen, with 90° angular distance between them, Figure 2b.

Due to the short time of impact loading, measuring and recording data are more complex than static loading, and the results recorded may be dependent on the approach used to measure the data. In the present study, to enhance measurement accuracy and quantity of the obtained results, three approaches were used to measure the specimens' deformation: (1) a high-speed video camera, (2) three strain gauges, and (3) two accelerometers. In the first method, a PHOTRON APX-RS camera with the recording capability up to 50,000 frames per second (fps) was used for measuring surface deformations of cylinders. The halogen lights were also placed to provide the lighting needed for recording high-speed videos. The high-speed video camera has recorded the impact process with a rate of 15,000 frames per second. Because of the camera's limitations, the recording window was decreased to 128×256 pixels (correspond
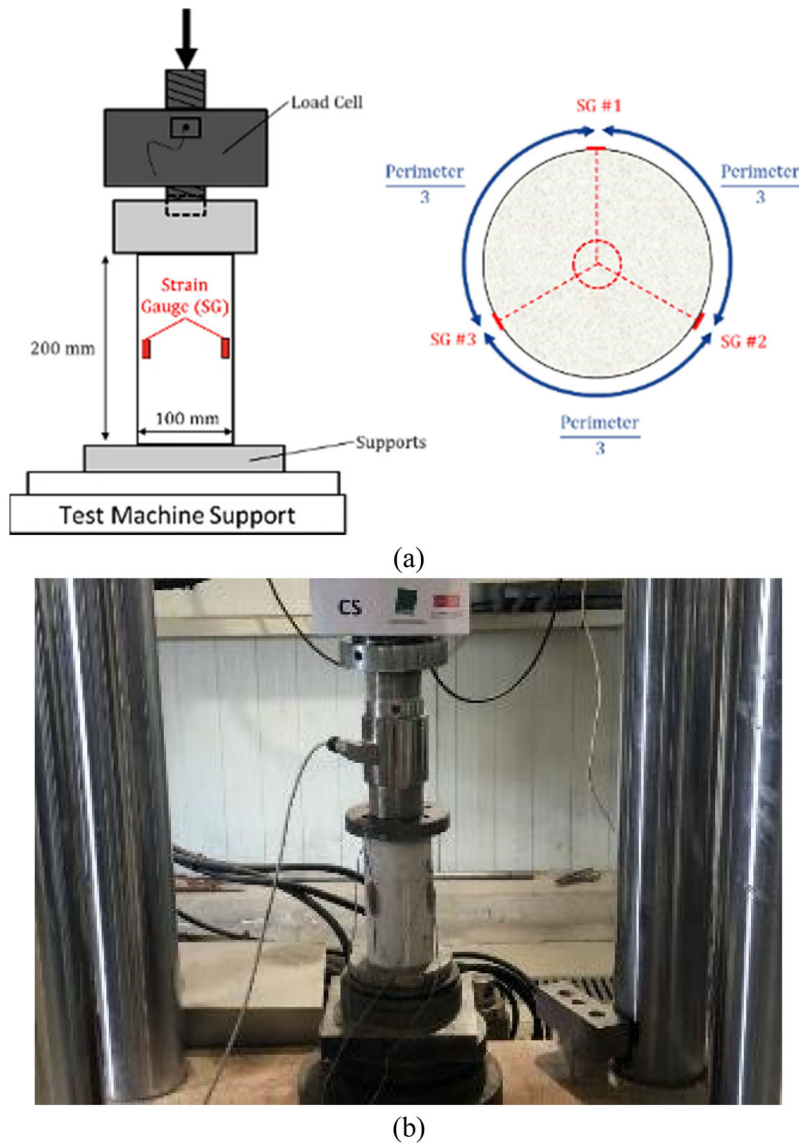
Figure 1. Test setup and monitoring system of a compression test: (a) Schematic representation including the position of the strain gauges (SG #1 to SG #3); and (b) image of the compression test and instrumented specimen.

**Table 3.** Groups of compression tests at different loading rate.

Specimen ID	Displacement rate [mm/min]	Drop height of impactor [mm]	Contact velocity [m/s]
S	1	–	–
Q10	10	–	–
Q100	100	–	–
Q500	500	–	–
HS1000	–	1000	4.42
HS1500	–	1500	5.42
HS2000	–	2000	6.26
HS2500	–	2500	7.00

to surface of $70 \times 35\,\text{mm}^2$ at the middle of cylinder), as shown in Figure 3, which depicts typical 1500 mms impact processes for specimen HS1500. Digital image correlation (DIC) was performed by GOM Correlate software to analyze the recorded videos. In addition to the average strain and strain rate acquired from the high-speed camera recordings, strain histories were also recorded by the strain gauges as mentioned above, which can be utilized to calculate the strain rate histories of the respective specimens.

In the second method, three strain gauges were placed around the mid height of cylindrical specimen, with 120° of angular distance, Figure 2a. Then, the strain gauges were connected to the data acquisition system. In the third method, the hammer velocity throughout the impact process $[\dot{\delta}(t)]$ was achieved by integrating the recorded acceleration by the accelerometers $[\ddot{\delta}(t)]$, Eq. (2). Afterward, average compressive deformation $[\delta(t)]$ was calculated by integrating of the velocity history, Eq. (3).
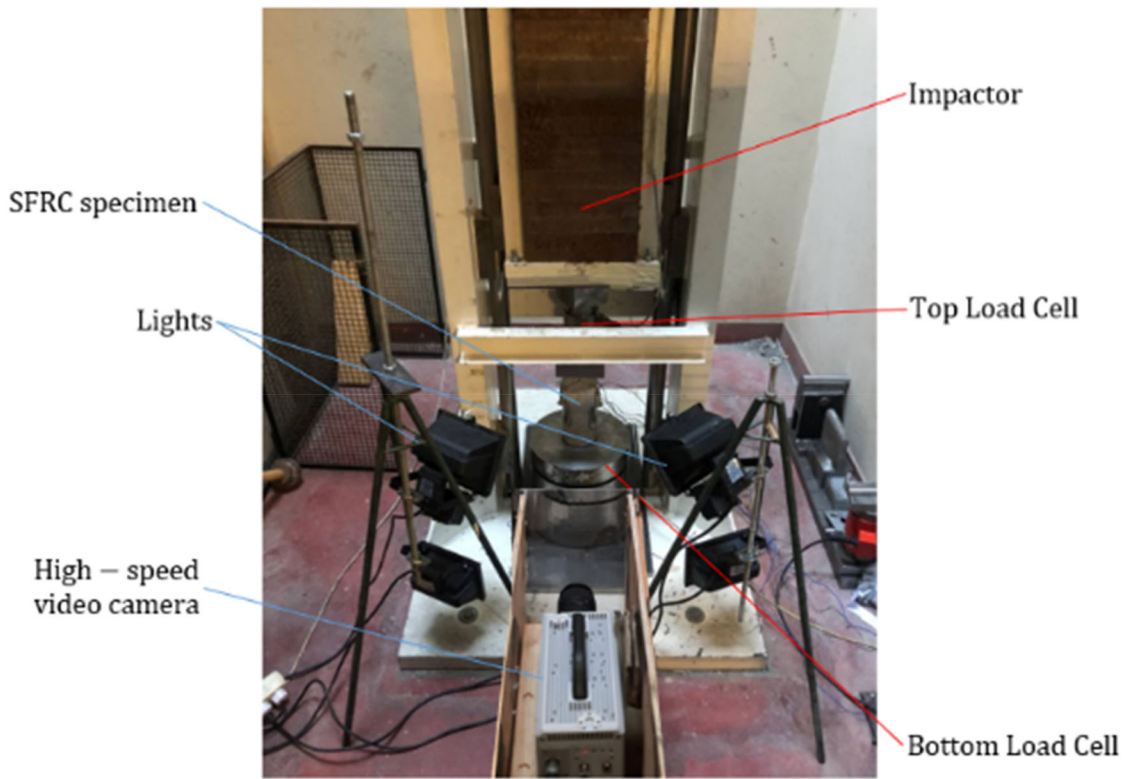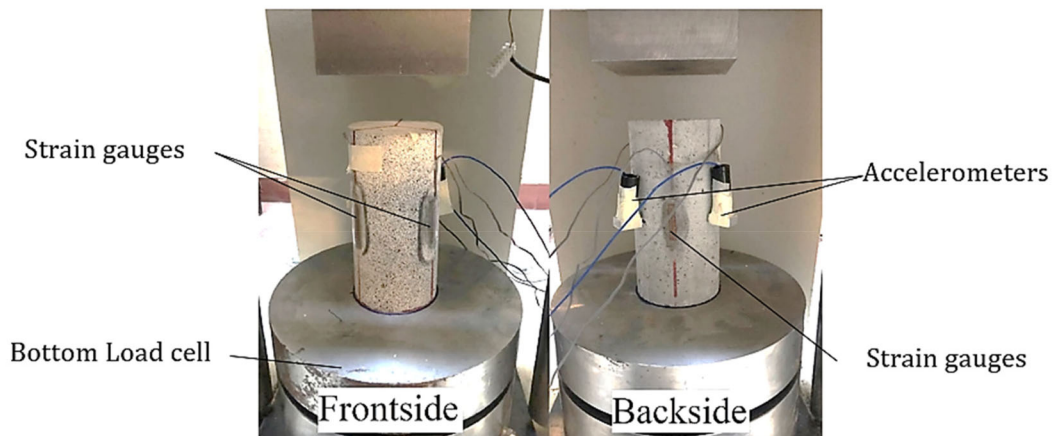
Figure 2. (a) Image of the drop weight impact device and (b) image of the cylinders before the impact test.

$$\dot{\delta}(t) = \int \ddot{\delta}(t) d(t) \qquad (1)$$

$$\delta(t) = \int \dot{\delta}(t) d(t) \qquad (2)$$

Totally, 17 cylindrical specimens have been tested under four different dropping heights, namely 2500, 2000, 1500, and 1000 mm, correspond to contact velocities of 7.00, 6.26, 5.42, and 4.43 m/s, respectively. The different drop heights were selected for determining the strain rate effect on the modulus of elasticity and compressive strength, and also for evaluating the variation of maximum acceleration and inertia force. In addition, the experimental data was also

compared to the proposed DIFs by CEB-FIP codes [29, 30] and other researchers [21, 25, 32, 33] that investigated the topic.

The deformation of a zone with 35 mm width and 70 mm height at the middle of the cylinder surface was measured. Analyzing the data collected showed that the deformation distribution along the 70 mm middle height of cylinder could be assumed linear and can be generalized for the height of cylinder (200 mm). Other researchers [34] also reported the same results. Since the deformation distribution shape follows the velocity and acceleration distribution, the assumption of the linear deformation distribution along the cylinder's height (by DIC results) can be also investigated by evaluating the acceleration distribution (by accelerometers).
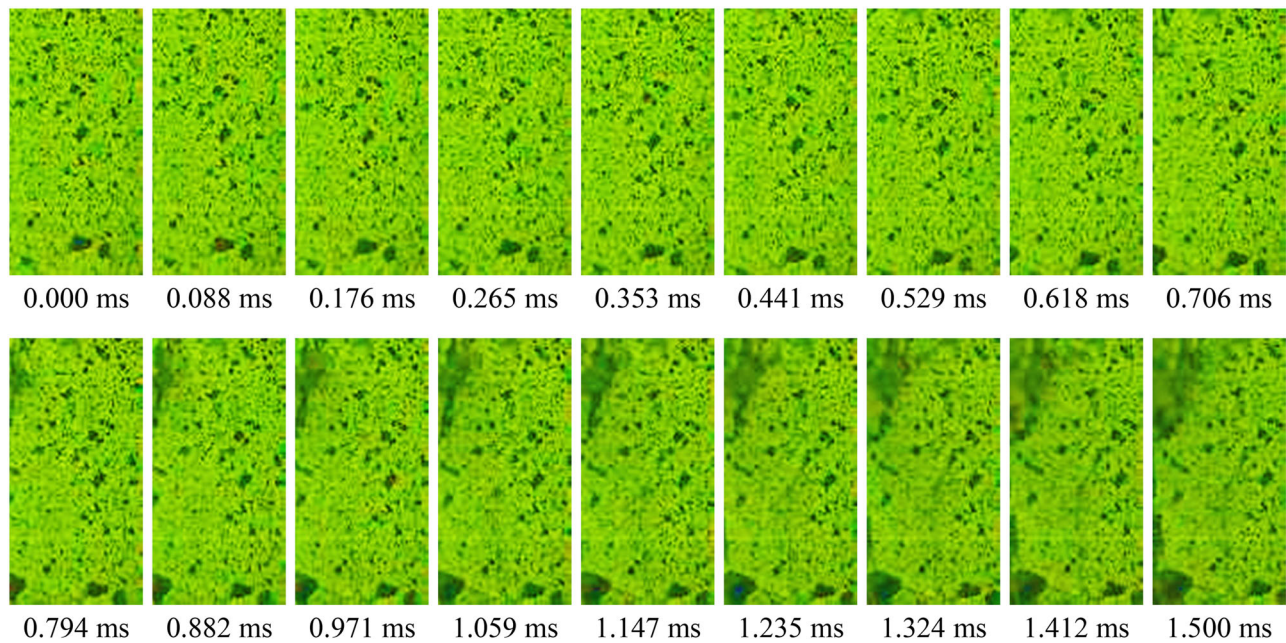
0.000 ms   0.088 ms   0.176 ms   0.265 ms   0.353 ms   0.441 ms   0.529 ms   0.618 ms   0.706 ms

0.794 ms   0.882 ms   0.971 ms   1.059 ms   1.147 ms   1.235 ms   1.324 ms   1.412 ms   1.500 ms

Figure 3. Typical captured frames using high-speed camera (cylinder HS1500-2).

Eight different points along the height of cylinders were considered to analyze the variation of acceleration, Figure 4a. Afterwards, using two accelerometers, the accelerations were sequentially measured in these eight points of specimen's height. The specimen was tested using a 20 kg impactor dropped from a height of 10 cm. Due to the limited number of accelerometers and the limited space required to use them, the values of acceleration at two points with same height (two sides of specimens, Accelerometer #1 and #2 in Figure 4a) are measured in each test. It means that, in total, 8 different tests are performed, and each was repeated five times. The average value of obtained accelerations at each height was considered to indicate the acceleration distribution along the cylinders' height. Though the results show an insignificant non-uniform axial acceleration, as shown in Figure 4a. Following the trend depicted in Figure 4a, a linear reduction acceleration was assumed from the top to the bottom of specimen along the axial direction. According to the acceleration and deformation distribution along cylinder's height, the value of acceleration at its mid-height was considered as the average acceleration, Figure 4b. Two acceleration values were considered for calculating the highest acceleration values obtained in the specimen: (a) highest acceleration at the top surface of cylinder in the contact point between cylinder and impactor ($\ddot{\delta}_{top}$), and (b) highest acceleration measured by the two accelerometers at the cylinder's mid-height ($\ddot{\delta}_{mid}$)that is assumed to be twice the value at mid height, if a linear axial distribution and zero acceleration at the bottom surface are assumed.

A linear distribution was assumed for deformation, velocity ($\dot{\delta}$), and acceleration ($\ddot{\delta}$) from the top to the bottom of the specimen, Figure 4b. This indicates that for a given time increment Δt, ($\Delta t = t_2 - t_1$), the deformation distribution is followed by the acceleration distribution along the cylinder's height [11].

3. Results and discussion

3.1. Fracture surfaces and failure patterns

As the SFRC was kept the same in all tested specimens with two flat and smooth surfaces (without use of Teflon), the loading strain rate applied in the performed experimental tests is the main parameter influencing the compressive failure mode observed. Under the quasi-static range, micro-cracks propagated parallel to the loading direction. After expanding the micro cracks corresponds to the nonlinear response in the pre-peak stage, the matrix cracks were appeared, and macro cracking occurred in the interface between the aggregate and mortar and also inside the mortar. Then these cracks were connected to each other along the height of cylinder. Under static loading, cracks propagated approximately in the axial direction and at the failure condition a shear failure mode was observed, Figure 5a. In this mode, the cylinders failed by splitting in the lateral sides. When the loading rate was increased, compressive barreling and columnar failure were also identified, in addition to the cone-shaped failure previously observed. These new failure modes resulted on an increase in the axial compressive force, Figure 5b–d.

Regarding impact loading, observations indicate that many micro cracks occurred and afterwards spread along height of the cylinders during testing. After testing, increasing in the number of fractured pieces was observed when the dropping height increases, Figure 5e–h. Increasing number of fractured pieces indicates a higher amount of energy dissipated during fracture. Moreover, the dominant failure mechanism was pull-out for the hooked end fibers in tested SFRC cylinders, Figure 6.

3.2. Compressive strain and strain rates

The ratio of the contact velocity of impactor to the length of the specimen is, in some cases, considered as an estimation of
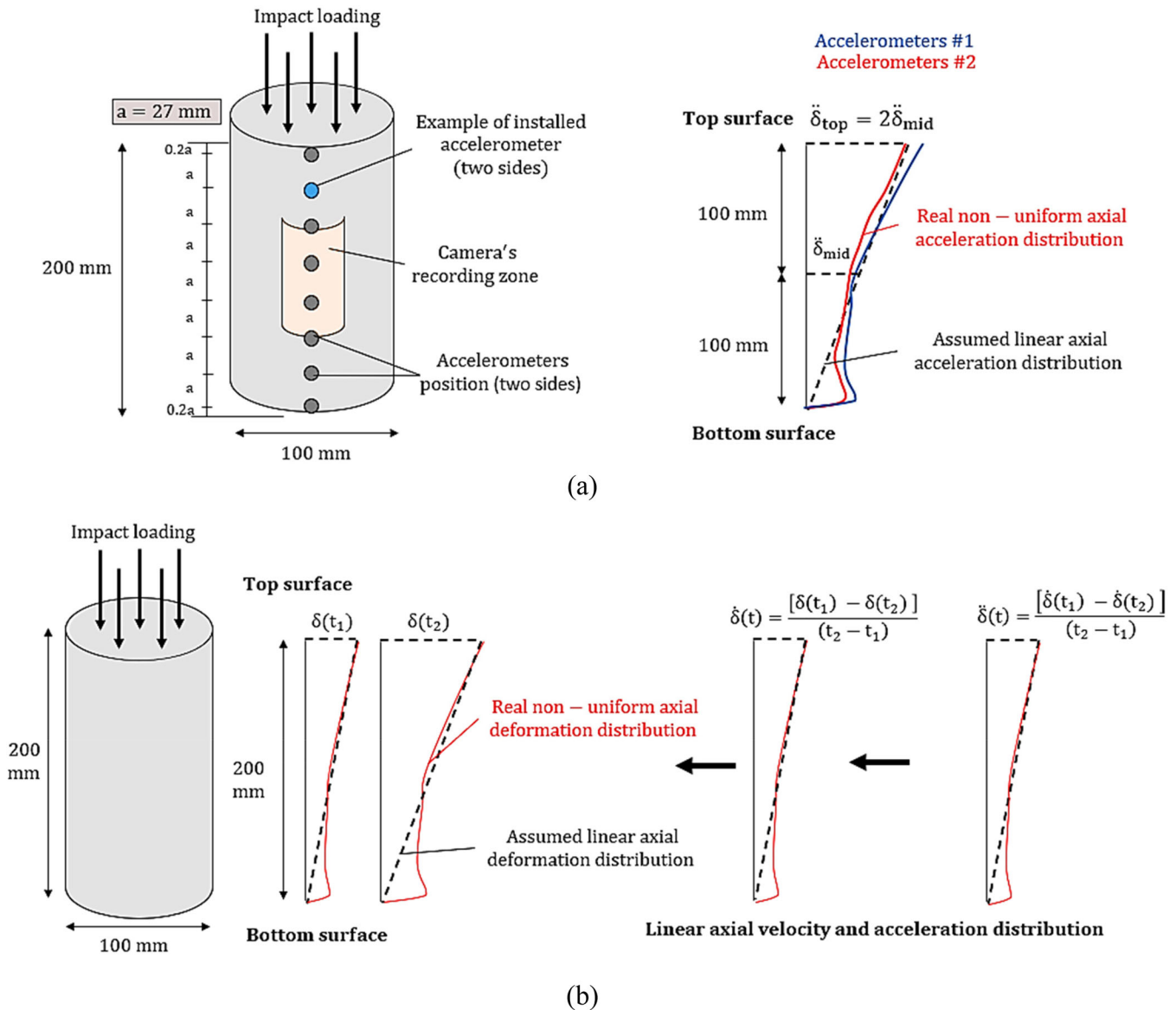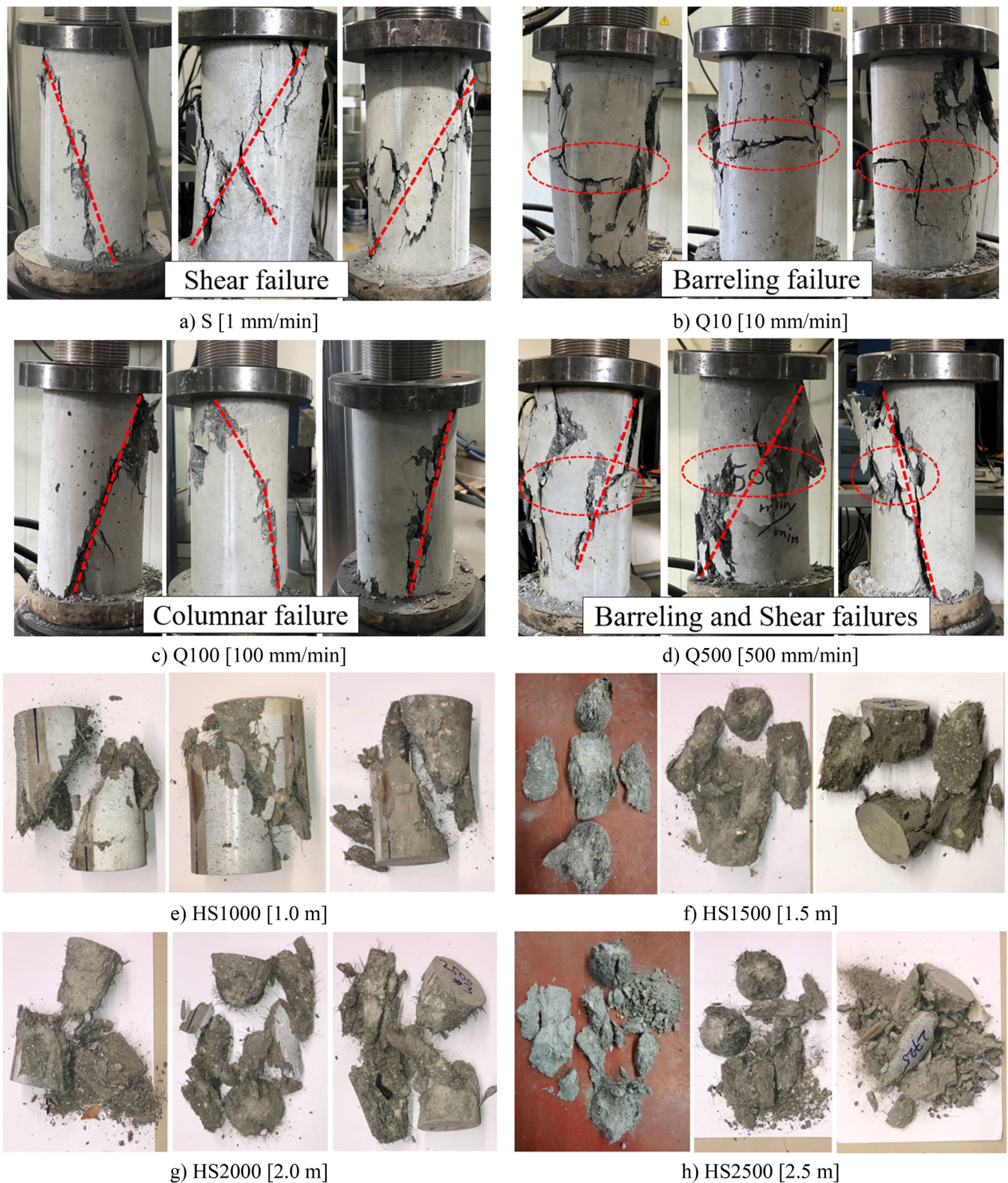
Figure 4. (a) Experimental acceleration distribution and (b) assumed linear distribution for acceleration, velocity, and deformation.

strain rate [17]. This value of strain rate was not consistent with the real strain rate developed in the specimen. Due to the difference between the stiffnesses of the impactor and the SFRC specimen, the specimen deformation velocity can be significantly different from the contact velocity of impactor. Consequently, the obtained strain rate from contact velocity of impactor was very different from the measured strain rate by strain gauges. For instance, Hjorth [35] reported that the strain rate calculated using contact velocity of impactor is much larger than the expected strain rate that can be obtained. The main reason of this difference is that the deformation velocity of specimen is smaller than the contact velocity of impactor. In the present study, three strain gauges were used to measure the strain during loading and, subsequently, the strain rate for each time step was calculated by averaging the recorded strain. In addition, digital image correlation (DIC) was utilized to estimate the strain at the mid height of the cylinders. The maximum compressive strain rate measured by both approaches (SG and DIC) during loading was considered as the strain rate of SFRC under impact loading, because the maximum strain rate is directly related to the specimen failure. The maximum compressive strain rate is also considered as the strain rate under impact by other researchers [15, 25, 28]. When using DIC, the deformation is measured in the central part of the specimens along a vertical line with a length of 70 mm positioned at middle of the specimen height. The recorded images were processed by a commercial DIC software (GOM Correlate-2D), using a normalized-sum-of-squared-difference correlation algorithm with an optimized 8-tap interpolation, for determining the strain distribution in the specimen. The average vertical compressive strain (ε_y) in specimens were obtained corresponding to average vertical compressive strain measured by the strain gauges with 30 mm of length at the mid height of cylinders. By calculating the vertical strain, the strain history was obtained considering the recording frame rate of camera (1500 fps). Figure 7a shows the strain versus time history obtained by the DIC directly measured from the specimen HS2500, as well as obtained by the strain gauges for specimen. As it was mentioned before, the acceleration distribution is non-uniform and thus the real deformation distribution is not

a) S [1 mm/min]

b) Q10 [10 mm/min]

c) Q100 [100 mm/min]

d) Q500 [500 mm/min]

e) HS1000 [1.0 m]

f) HS1500 [1.5 m]

g) HS2000 [2.0 m]

h) HS2500 [2.5 m]

Figure 5. Failure patterns of SFRC specimens under quasi-static loading (a–d) and impact loading (e–h).

uniform along the cylinder and there are differences between the strain rates obtained with strain gauges and with DIC. As shown in Figure 7a, due to the limitation in the recording frame rate, the number of data obtained by DIC is lower than the by SGs. Nevertheless, the graph presented in Figure 7b indicates an acceptable correlation between the strain rate obtained by DIC and the strain rate recorded by strain gauges.

3.3. The inertia force generated by impact loading

Figure 8 depicts the time variation of reaction and impact forces for one representative specimen for each dropping height.

The time delay between the onset of the reaction and the impact forces are 80, 99, 121, and 134 μs, which correspond
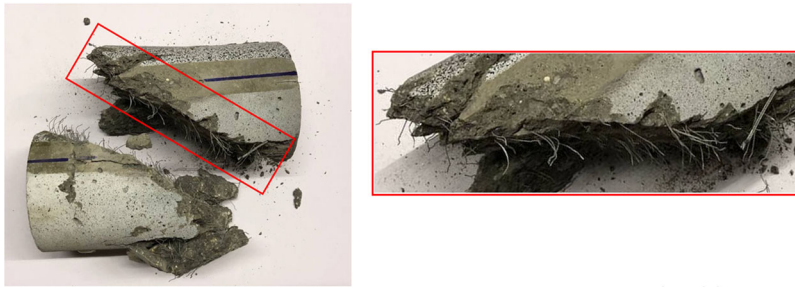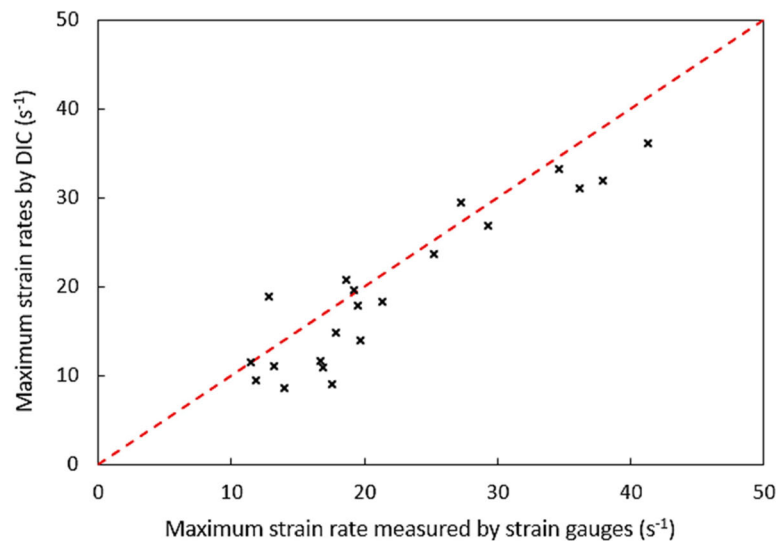
Figure 6. Pull-out mechanism for the hooked end fibers.
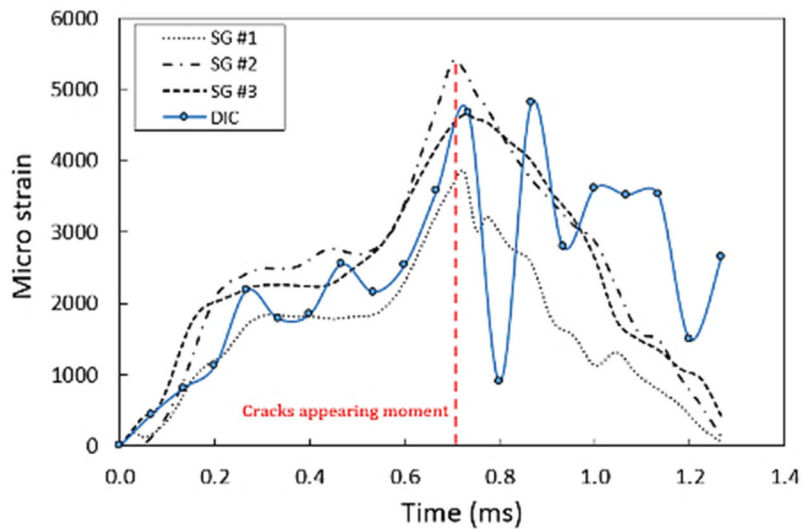
(a)

(b)

Figure 7. (a) Strain-time history estimated by DIC and from strain gauges for specimen HS2500; (b) maximum strain rates estimated by DIC and from strain gauges.

to dropping heights of 2500, 2000, 1500, and 1000 mm, respectively. Thus, the time interval between reaction and impact has decreased with the increase of the drop height of the impactor. The time gap between bottom and top load cells could be related to propagation of stress wave along the cylinders. Due to limitations of load cell, the maximum impact load in four tested samples could not be measured, Table 4.

Based on the results under impact loading, different forces values were recorded by the bottom and top load cells, which confirms the importance of the inertia force. As it is known, the inertia force value depends on the acceleration values along the cylinder. The results indicated that the ratio of inertia to impact force is significantly dependent on the acceleration, Table 4. Similar observation was also
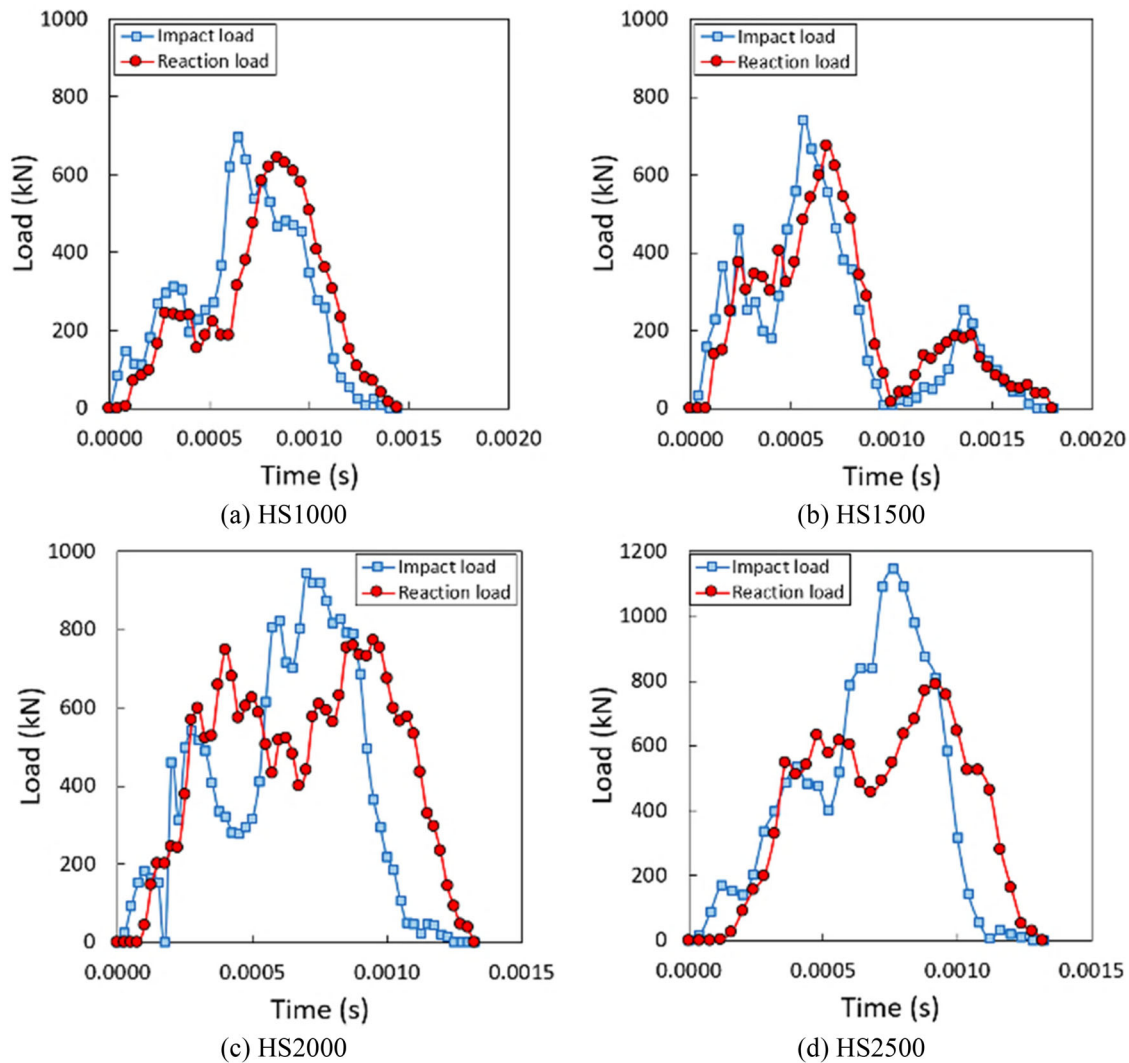
Figure 8. Impact and reaction forces *vs.* time during impact loading.

Table 4. Strain rate effect on maximum acceleration and the inertia force.

Specimen ID	Strain rate [s⁻¹]	Mass (m) [kg]	Reaction force [kN]	Impact force [kN]	Experimental inertia force [kN]	Inertia to impact force ratio (ω)	$\ddot{\delta}_{max,\,top}$ [gᵃ]	$\ddot{\delta}_{max,\,mid}$ [gᵃ]	Analytical inertia force, Eq. (8) [kN]
HS1000-1	10.80	3.63	643.8	697.2	53.3	0.077	1662	831	20.1
HS1000-2	8.39	3.75	648.3	699.8	51.5	0.074	1974	987	24.7
HS1000-3	9.41	3.71	662.5	700.2	37.6	0.054	1482	741	18.3
HS1000-4	10.15	3.61	681.2	749.7	68.4	0.092	2026	1013	24.4
HS1500-1	18.65	3.75	671.8	nr	nr	nr	nr	nr	nr
HS1500-2	25.18	3.68	689.5	769.6	80.1	0.105	2974	1487	36.5
HS1500-3	19.50	3.72	695.9	753.5	57.7	0.077	2678	1339	33.2
HS1500-4	21.22	3.75	674.4	740.8	66.1	0.090	2540	1270	31.8
HS2000-1	29.28	3.61	704.2	872.7	168.5	0.196	3148	1574	37.9
HS2000-2	36.17	3.72	772.6	945.0	172.4	0.185	3018	1509	37.4
HS2000-3	34.60	3.73	714.2	933.6	219.4	0.239	3222	1611	40.1
HS2000-4	24.65	3.72	757.6	nr	nr	nr	3380	1690	41.9
HS2500-1	27.27	3.74	788.3	1146.7	358.4	0.319	6346	3173	79.1
HS2500-2	37.94	3.74	831.3	nr	nr	nr	4128	2064	51.5
HS2500-3	35.83	3.64	797.1	nr	nr	nr	5756	2878	69.8
HS2500-4	39.21	3.66	846.0	nr	nr	nr	6236	3118	76.1

nr: not recorded.
ᵃg = 9.81 m/s².

stated by Xu et al. [15]. The measured accelerations using two positioned accelerometers in the middle of the cylinders' height indicated that values of acceleration and consequently inertia force increase as the impactor dropping height increases. The maximum acceleration measured is taken as the acceleration of the specimens, since the maximum acceleration is closely related to the maximum inertia force. The maximum acceleration values obtained for drop heights of

impactor of 2500, 2000, 1500, and 1000 mm, were 3173, 1611, 1487, and 1013 g, respectively, and the ratio of inertia to impact force (ω) was 32%, 24%, 10%, and 9%, respectively, as shown in Table 4.

The equation of motion can be used to calculate the inertia force analytically. Based on the structural dynamic theory, in the relatively motion of an element from a reference, the inertia forces are proportionate to its amount of acceleration in the same axis with opposite orientation [36]. The inertia force is directly dependent on amount of the acceleration. Consequently, inertia force increases by increasing the value of applied acceleration. Based on the motion equation, the inertia force is a function of mass and acceleration of specimen:

$$\sum F = F_i = F_t - F_b = m\ddot{\delta}_{\max} \tag{3}$$

where F_t, F_i, F_b, $\ddot{\delta}_{\max}$, and m are the impact force (measured on top), the inertia force, the reaction force (measured on bottom), maximum acceleration, and mass of specimen, respectively. The motion of particles in the instrumented drop weight test is limited for deforming in the direction of loading, hence only the inertia force mobilized in the loading direction is calculated. An evaluation of axial inertia effects for impact loading was given in Figure 9, by considering the impact force measured on top of the specimen (F_t), and the inertial response along the length of the specimen.

By assuming a linear displacement profile (or uniform strain) along the specimen, the strain is just time dependent, [$\varepsilon(t)$]. Accordingly, the inertia force in an element ($A.dx$) is:

$$\delta F_i = \rho A dx \left(\ddot{\delta}_{\max, top} \right) \left(\frac{x}{h} \right) \tag{4}$$

where ρ, A, and h are the mass density, the cross section area, and the height of the cylinder, respectively [17]. $\ddot{\delta}_{\max, top}$ is the maximum values of acceleration at the top of cylinder, contact between cylinder and impactor that was extrapolated by the value measured in the accelerometer placed at middle height of the cylinder and assuming null

acceleration in the bottom of the specimen, Figure 9. A virtual displacement at the top of the specimen (δu_t) is imposed where the compressive force is applied. The virtual work (W) performed by the inertia force on the element ($A.dx$) is:

$$dW = \rho A dx \left(\frac{\ddot{\delta}_{\max, top} x}{h} \right) \left(\frac{\delta u_t x}{h} \right) = \frac{\rho A \ddot{\delta}_{\max, top} \delta u_t x^2}{h^2} dx \tag{5}$$

and then the total virtual work done by the inertia force along the entire length of the specimen can be given by:

$$W = \int_0^h \frac{\rho A \ddot{\delta}_{\max, top} \delta u_t x^2}{h^2} dx = \frac{\rho A h \ddot{\delta}_{\max, top} \delta u_t}{3} \tag{6}$$

Then, the inertia force can be obtained by Eq. (8), based on the virtual work principle ($F_i \delta u_t$):

$$F_i = \rho A (h/3) \ddot{\delta}_{\max, top} \tag{7}$$

For evaluation the relation between maximum acceleration and inertia force, the maximum acceleration at the cylinder's mid height ($\ddot{\delta}_{\max, mid} = 0.5 \ddot{\delta}_{\max, top}$) was considered, as an input to the motion equation. The analytical inertia force has been calculated assuming a linear acceleration distribution along the cylinders' height, Eq. (8). By comparing the experimental to calculated analytical inertia forces, it can be found that by increasing the strain rate (or impactor dropping height), the analytical equation underestimates the inertia force, Figure 10a. This means that when the contact velocity is high (higher drop height of the impactor), the acceleration distribution along the cylinder's height is non-linear. In another word, in the higher contact velocity, the effect of the measurement location of acceleration on the maximum acceleration is higher. The obtained profile acceleration along recorded zone by DIC (middle 70 mm of cylinder's height) approves increasing of non-linearity of acceleration distribution along the cylinder's height with contact velocity, Figure 11. The values of acceleration (average of four specimens for each drop height of impactor)
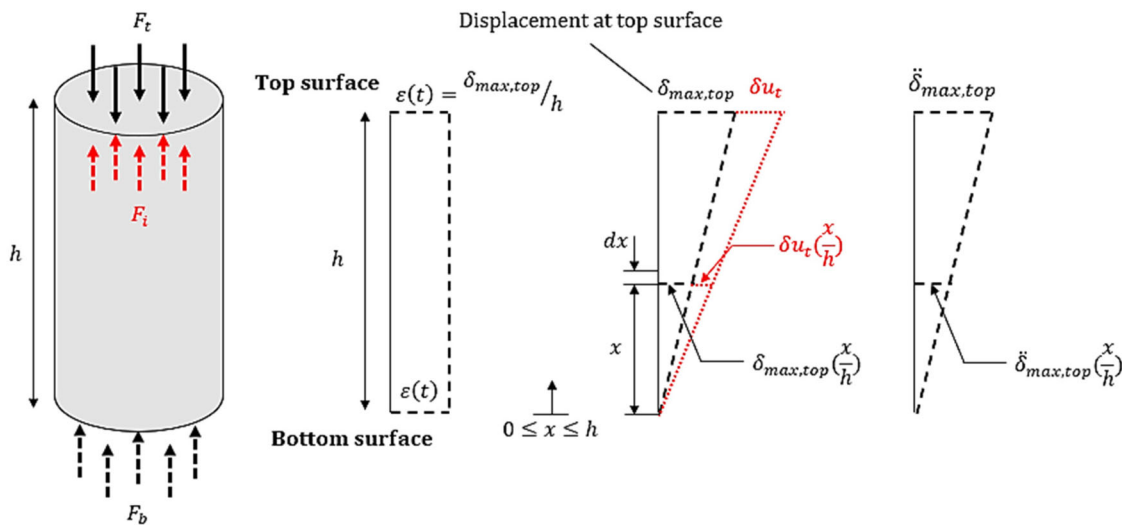

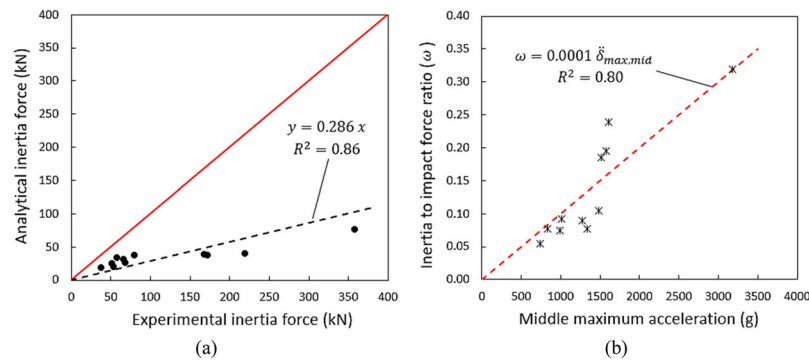**Figure 9.** Evaluation of inertia effect for impact loading.

Figure 10. (a) Comparing of analytical and experimental inertia force, (b) inertia to impact force ratio versus middle maximum acceleration.
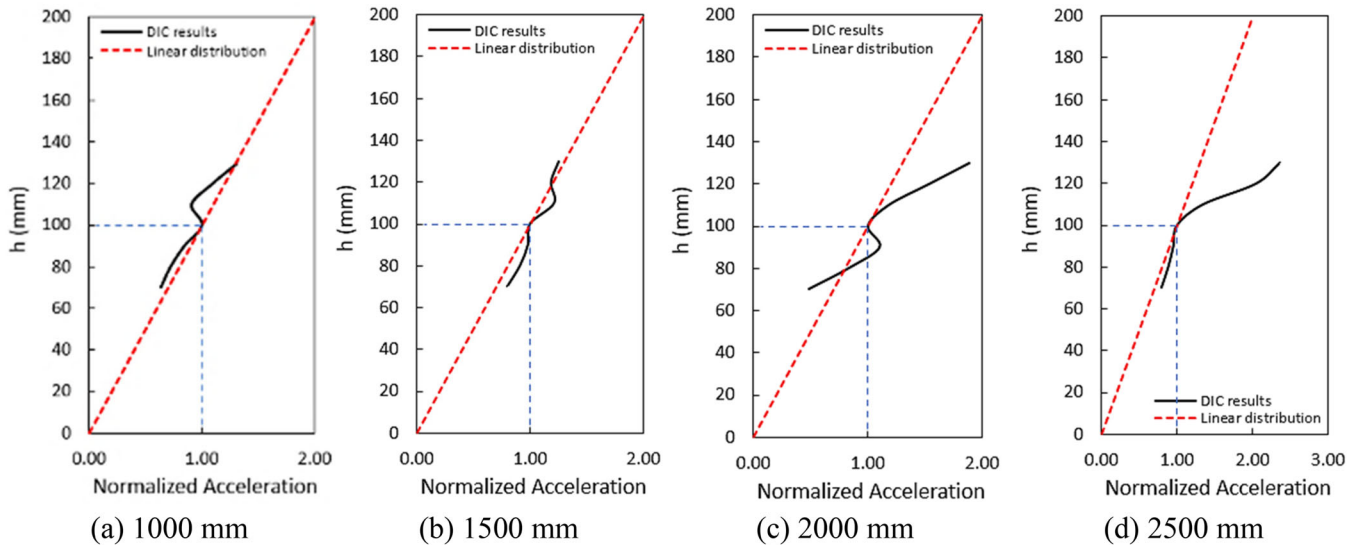

Figure 11. Normalized acceleration distribution to middle acceleration along recorded zone by DIC at different dropping heights of impactor.

were normalized to the middle maximum acceleration for each drop height of impactor to make a better comparison. This non-linearity acceleration distribution is more obvious in specimens of HS2000 and HS2500, Figure 11. As a result, a real non-linear acceleration distribution can be assumed to modify the inertia force value calculated by the motion equation.

When the maximum acceleration increases, the inertia to impact force ratio increases in an approximately linear trend, as shown in Figure 10b. The effect of inertia is amplified with increase of the impactor dropping height. Similar findings have been reported in Banthia and Mindess [11] and Xu et al. [15].

3.4. Stress-strain curve at different strain rates

The compressive stress-strain curves measured in all the SFRC cylinders tested in the range of quasi-static were demonstrated in Figure 12. To omit the effect of inertia on material properties, the reaction force was used in this study to calculate the compressive strength of SFRC under impact loading, which is consistent with Xu et al. [15] and Bischoff and Perry [17]. Therefore, the compression stress was calculated considering the force recorded by the bottom load-cell, and the compression strain was determined by taking the

average value obtained from the three installed strain gauges at the middle of the SFRC cylinders height.

In the impact tests, the reaction force was considered to obtain the compressive stress neglecting the effect of inertia. For deriving the stress-strain curve, first, the time delay between the recorded reaction force and the measured strain was removed. Then the average of three strain curves (obtained from SG#1 to #3) up to peak strain was considered and the post peak stage of recorded strain history was ignored. Because the compressive loading was applied in one direction and decreasing the value of strain cannot be acceptable. Afterward, for each time step, both stress and strain were available. Subsequently, the stress-strain relations of SFRC for the different dropping height of the impactor were obtained by synchronizing the stress-time curve and the average strain-time curve, Figure 13. Since during measured strain history the value of stress experiences a peak, the results have shown some post-peak stage in the stress-strain curve.

The loading time at peak strain for the impactor dropping heights of 1000, 1500, 2000, and 2500 mm is shown in Figure 14, where it is visible that it decreases with the increase the dropping height of the impactor. This is due to an increase of both the contact velocity and the deformation rate along the specimen.
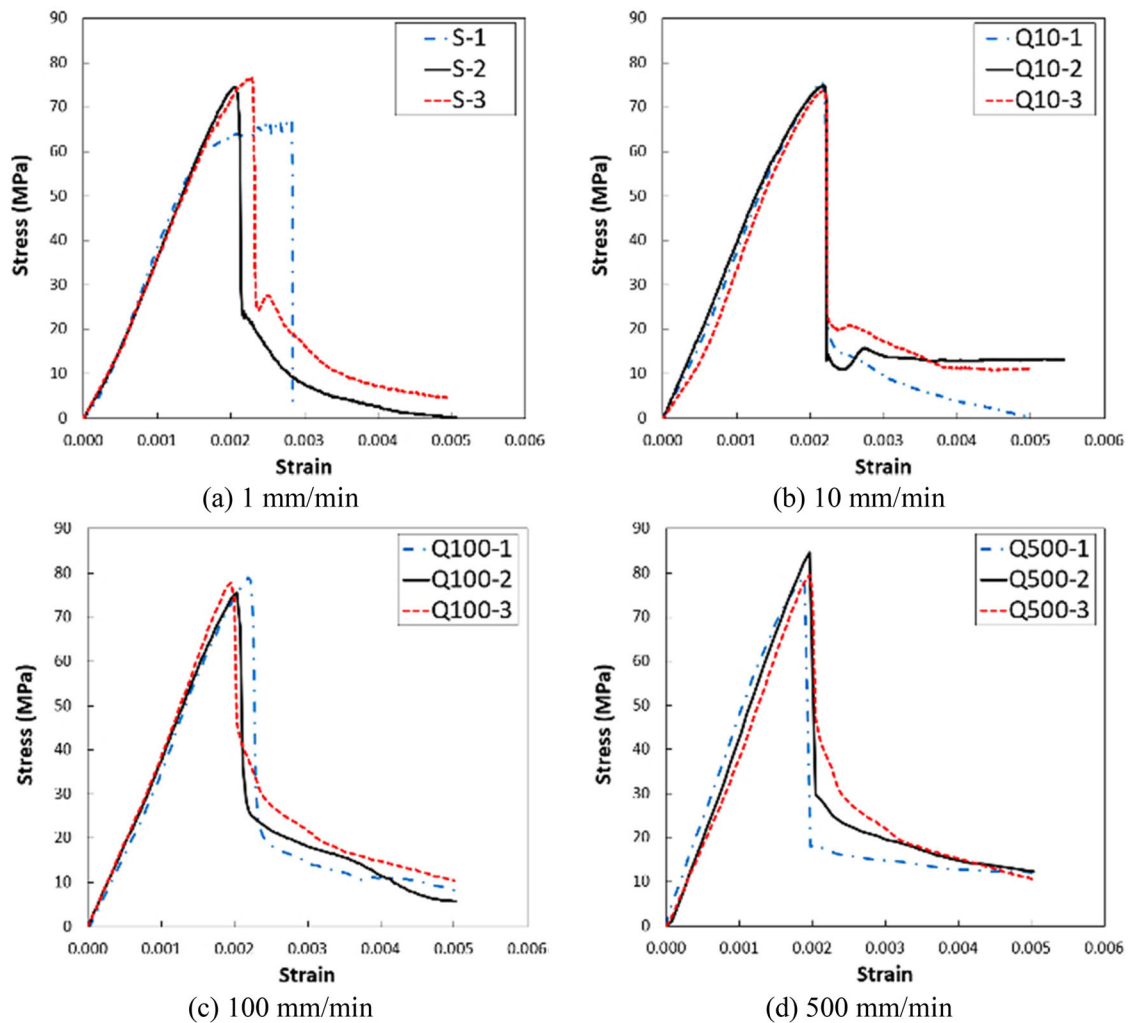
Figure 12. Stress-strain curves registered in the quasi-static loading tests at different displacement rates.

3.5. Effect of strain rate on the compression behavior of SFRC

3.5.1. Compressive strength and Young's modulus

In the present research, the maximum reaction force was considered in the calculation of the SFRC compressive strength. The compressive strain was obtained by computing the average of the aforementioned three strain gauges. The mechanical results obtained for the specimens tested at the lowest strain rate are shown in Table 5. Three specimens were tested at the quasi-static compressive strain rate of $1.33\mathrm{E}-05\,\mathrm{s}^{-1}$. In the present study, toughness is the total area under the stress-strain curve up to failure.

Twenty-nine cylinders were tested to determine the strain rate effect on the modulus of elasticity and compressive strength. The results obtained are shown in Table 6. They evidence that the compressive strength, the modulus of elasticity, and the toughness of SFRC specimens are sensitive to the imposed strain rate. The DIF of compressive strength (DIF_C), modulus of elasticity (DIF_Y), and toughness (DIF_T) for each specimen were calculated and compared with existing DIF models to investigate which one can better predict the effect of strain rate on the properties of the developed SFRC.

The modulus of elasticity and compressive strength increased with the strain rate. In Figure 15, the values of strain rate are represented in a logarithmic scale, and the relationship between DIF and strain rate was demonstrated utilizing a log-linear graph. For the considered range of quasi-static strain rates, an almost linear relationship was obtained between the logarithmic values of strain rate applied and the corresponding DIF values for the modulus of elasticity and compressive strength of SFRC. Furthermore, the evolution of DIF is different for modulus of elasticity and compressive strength. The models proposed by CEB-FIP [29, 30], which are applicable to both plain concrete and SFRC, describe quite well the DIF of compressive strength of SFRC, at the measured strain rate range, but underestimate the modulus of elasticity at the higher strain rates. It must be noted that both CEB-FIP models [29, 30] use the same equation to estimate the DIF of the modulus of elasticity.

The DIF values for the compressive strength were also evaluated considering the models proposed by Hao and Hao [25], Fujikake et al. [33], and Krahl et al. [37], Table 7. Hao and Hao [25] proposed a model based on experimental results obtained with spiral fibers and SHPB testing.
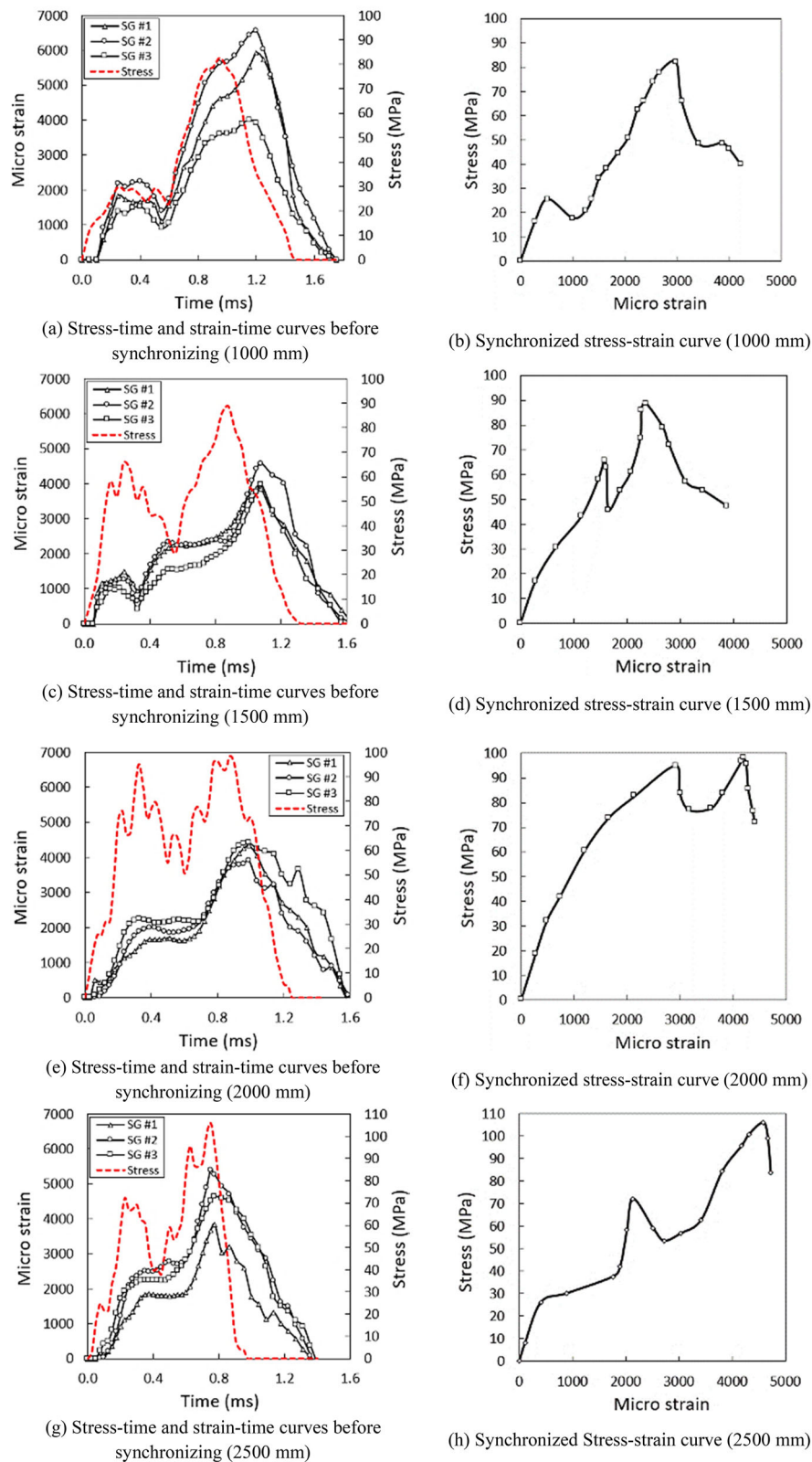
Figure 13. Typical stress and strain histories and stress-strain curve at different drop heights of impactor.

Fujikake et al. [33] proposed a constitutive model for the dynamic compressive strength of concrete materials under high-strain rates. Krahl et al. [37] proposed an alternative model based on experimental results obtained using smooth steel fibers. The experimental DIF values for the compressive strength of SFRC ranged between 1.02 and 1.48. The results

registered in HS2500-5 specimen are out of this range, as shown in Figure 15a, and therefore this specimen was considered as an outlier. The maximum DIF obtained for the modulus of elasticity was 1.63. As shown in Figure 15, the CEB-FIP models [29, 30] predict the increase of compressive strength more precisely than the other considered models,
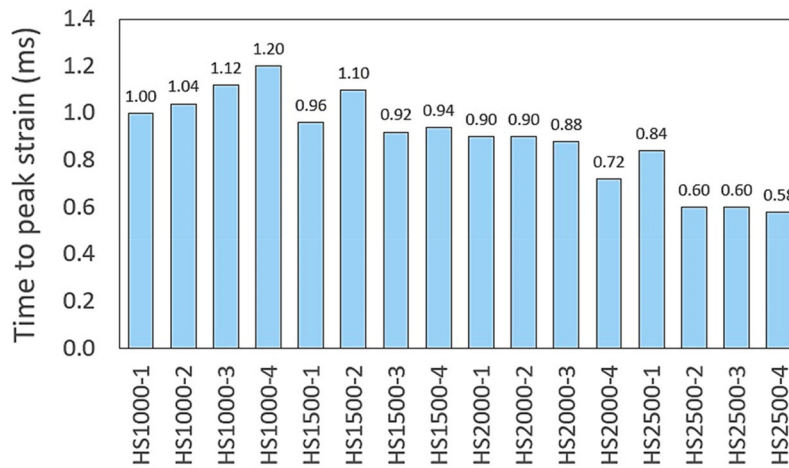
Figure 14. Compressive strain histories at different dropping heights of impactor.

Table 5. Cylindrical specimens tested at quasi-static strain rate (1.33E-05 s^{-1}).

Type ID	Compressive strength [MPa]	Modulus of elasticity [GPa]	Toughness [kJ/m^3]
S-1	73.07	41.72	99.96
S-2	76.72	42.40	124.24
S-3	67.09	40.55	126.28
Average	72.29 (5.5)	41.56 (1.8)	116.83 (10.2)

Note: Values in parentheses are the coefficient of variation (in percentage).

Table 6. Summary of quasi-static and impact test results of SFRC specimens.

Type ID	Strain rate [s^{-1}]	Compressive strength [MPa]	Modulus of elasticity [GPa]	Toughness [kJ/m^3]	DIF (f_c)	DIF (E_c)	DIF (T)
S (average)	1.33E − 05	72.29	41.56	116.83	1.000	1.000	1.000
Q10-1	1.33E − 04	75.65	42.21	102.74	1.047	1.080	0.879
Q10-2	1.33E − 04	74.83	42.39	122.28	1.035	1.086	1.047
Q10-3	1.33E − 04	73.68	43.06	125.14	1.019	1.103	1.071
Q100-1	1.33E − 03	76.97	43.04	120.45	1.092	1.170	1.031
Q100-2	1.33E − 03	75.55	42.08	114.24	1.045	1.146	0.978
Q100-3	1.33E − 03	77.91	43.32	127.75	1.078	1.179	1.093
Q500-1	6.67E − 03	76.03	43.83	126.40	1.093	1.194	1.082
Q500-2	6.67E − 03	74.58	44.51	137.93	1.170	1.212	1.181
Q500-3	6.67E − 03	79.53	44.19	130.10	1.100	1.204	1.114
HS1000-1	10.80	81.98	52.70	141.40	1.125	1.268	1.210
HS1000-2	8.39	82.55	53.00	153.90	1.133	1.275	1.317
HS1000-3	9.41	84.36	52.10	156.70	1.158	1.254	1.341
HS1000-4	10.15	86.74	55.60	154.70	1.190	1.338	1.324
HS1500-1	18.65	85.58	61.40	166.50	1.174	1.478	1.425
HS1500-2	25.18	87.83	59.63	207.40	1.205	1.435	1.775
HS1500-3	19.50	88.64	52.40	185.50	1.217	1.261	1.588
HS1500-4	21.22	85.87	58.80	163.40	1.179	1.415	1.399
HS2000-1	29.28	89.71	59.26	212.53	1.231	1.426	1.819
HS2000-2	36.17	98.43	63.29	285.03	1.351	1.523	2.440
HS2000-3	34.60	90.98	65.46	216.58	1.249	1.575	1.854
HS2000-4	24.65	96.46	60.30	215.40	1.324	1.451	1.844
HS2500-1	27.27	100.42	60.91	227.79	1.378	1.466	1.950
HS2500-2	37.94	105.89	67.77	286.51	1.453	1.631	2.452
HS2500-3	35.83	101.54	61.47	240.67	1.393	1.479	2.060
HS2500-4	39.21	107.72	65.70	296.90	1.478	1.581	2.541
HS2500-5[a]	41.34	143.08	67.82	240.74	1.961	1.629	2.453

[a]The obtained results from specimen HS2500-5 were considered as outliers.

both in quasi-static and in impact range of strain rate. The differences among the proposed models can be attributed to the fact that the strain rate sensitivity of SFRC is rather influenced by parameters such as fibers shape, fibers volume fraction, fibers aspect ratio, tensile strength of steel fibers, and type of test for compressive loading (either Instrumented Drop Weight Test or SHPB test).

Figure 16 compares the experimental results obtained in the present research and those found in the literature [15, 18, 19, 21, 25, 28, 37, 39–47]. The obtained results are, in general, in agreement with the ones obtained by other authors, where after a smooth increase of the compressive strength up to a strain rate of about 1 and 20 s^{-1}, an abrupt increase was observed correspond to the obtained results using drop weight impact and SHPB, respectively. Nevertheless, more experimental results are required for assessing the effect of the shape and volume fraction of the steel fibers on the DIF of the compressive strength of SFRC.
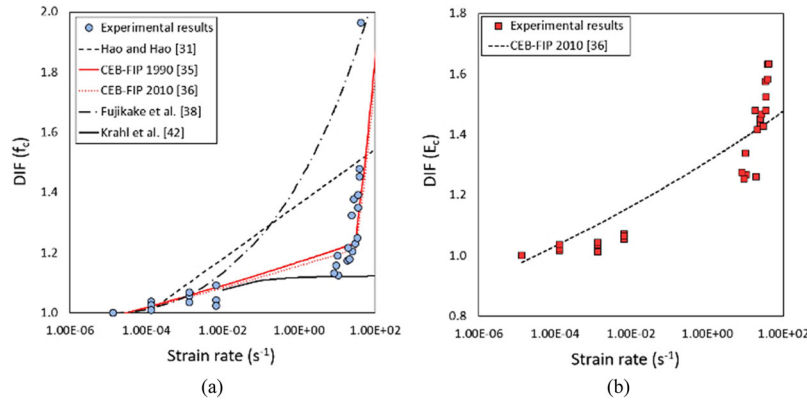
Figure 15. DIF of (a) compressive strength and (b) modulus of elasticity of SFRC.

Table 7. Previously proposed empirical models for dynamic increase factor.

Parameter	Reference	Model
DIF (f_c)	CEB-FIP design code [29]	$DIF(f_c) = \begin{cases} \left(\frac{\dot{\varepsilon}_c}{\dot{\varepsilon}_{cs}}\right)^{1.026\alpha}, & \dot{\varepsilon}_c \leq 30\,\text{s}^{-1} \\ \gamma\left(\frac{\dot{\varepsilon}_c}{\dot{\varepsilon}_{cs}}\right)^{1/3}, & \dot{\varepsilon}_c > 30\,\text{s}^{-1} \end{cases}$ $\alpha = (5 + 0.9f'_c)^{-1}$, $\log(\gamma) = 6.156\alpha - 2$, $\dot{\varepsilon}_{cs} = 30 \times 10^{-6}\,\text{s}^{-1}$
	CEB-FIP model code [30]	$DIF(f_c) = \begin{cases} \left(\frac{\dot{\varepsilon}_c}{\dot{\varepsilon}_{cs}}\right)^{0.014}, & \dot{\varepsilon}_c \leq 30\,\text{s}^{-1} \\ 0.012\left(\frac{\dot{\varepsilon}_c}{\dot{\varepsilon}_{cs}}\right)^{1/3}, & \dot{\varepsilon}_c > 30\,\text{s}^{-1} \end{cases}$, $\dot{\varepsilon}_{cs} = 30 \times 10^{-6}\,\text{s}^{-1}$
	Hao and Hao [25]	$DIF(f_c) = \begin{cases} 0.0672(\log\dot{\varepsilon}_c) + 1.2688, & v_f = 0.0\% \\ 0.0679(\log\dot{\varepsilon}_c) + 1.2716, & v_f = 0.5\% \\ 0.0907(\log\dot{\varepsilon}_c) + 1.3628, & v_f = 1.0\% \end{cases}$
	Krahl et al. [37]	$DIF(f_c) = \left(0.89 + v_f\left(\frac{\dot{\varepsilon}_c}{\dot{\varepsilon}_{cs}}\right)^{-0.49}\right)^{-1}$
	Fujikake et al. [33]	$DIF(f_c) = \left(\frac{\dot{\varepsilon}_c}{\dot{\varepsilon}_{cs}}\right)^{0.006\left[\log\left(\frac{\dot{\varepsilon}_c}{\dot{\varepsilon}_{cs}}\right)\right]^{1.05}}$, $\dot{\varepsilon}_{cs} = 12 \times 10^{-6}\,\text{s}^{-1}$
DIF (E_c)	CEB-FIP model code [30]	$DIF(E_c) = \left(\frac{\dot{\varepsilon}_c}{\dot{\varepsilon}_{cs}}\right)^{0.026}$, $\dot{\varepsilon}_{cs} = 30 \times 10^{-6}\,\text{s}^{-1}$
DIF (T)	Ibrahim et al. [38]	$DIF(T) = \text{Exp}\left[2.6 \times 10^{-7}\left(\frac{\dot{\varepsilon}_c}{\dot{\varepsilon}_{cs}}\right)\left(1 + 1.07RI_v^{0.011}\right)\right]$, $RI_v = v_f\frac{l}{d}$

$\dot{\varepsilon}_c$ and $\dot{\varepsilon}_{cs}$ are applied strain rate and reference strain rate correspond to static loading, respectively. f_c is the compressive strength. v_f, l, and d are volume fraction, length, and diameter of steel fiber.

The results obtained from the compressive quasi-static, drop weight impact, and SHPB tests, show that in addition to the range and values of strain rate, the type of test setup (the way the load is applied) plays an important role in the effect of strain rate on the compressive characteristics of SFRC such as compressive strength, modulus of elasticity, and toughness. As can be seen in Figure 16, the values of strain rate obtained from SHPB tests are often higher than drop weight impact test and the lowest obtained strain rate in the impact range in the SHPB test is also higher than drop weight impact test. Furthermore, due to different approaches for applying impact loading, the increasing trend of modulus of elasticity and compressive strength with the strain rate using the SHPB test is not the same as the drop weight impact test, Figure 16. As a result, the proposed relations must consider the type of loading (test approach) in addition to the strain rate and accordingly predict the values of compressive strength and modulus of elasticity. For this purpose, in this study, an empirical relationship was proposed for each type of load and each mechanical characteristic to explain the strain rate sensitivity of SFRC. Three different models were proposed for predicting each mechanical characteristic; one model in the range of quasi-static and two

models in the range of impact correspond to the SHPB and drop weight impact tests.

$$DIF_{Quasi-Static} = \left(\frac{\dot{\varepsilon}_c}{\dot{\varepsilon}_{cs}}\right)^{A \times 10^{-3}}, \quad \dot{\varepsilon}_c \leq \dot{\varepsilon}_{tr} \quad (8)$$

$$DIF_{Drop\,weight} = B \times 10^{-7}\left(\frac{\dot{\varepsilon}_c}{\dot{\varepsilon}_{cs}}\right) + C, \quad \dot{\varepsilon}_c > \dot{\varepsilon}_{tr} \quad (9)$$

$$DIF_{SHPB} = D.\left[\log\left(\dot{\varepsilon}_c/\dot{\varepsilon}_{cs}\right)\right]^2 + E.\left[\log\left(\dot{\varepsilon}_c/\dot{\varepsilon}_{cs}\right)\right] + F, \quad \dot{\varepsilon}_c > \dot{\varepsilon}_{tr} \quad (10)$$

where $DIF_{Quasi-Static}$, $DIF_{Drop\,weight}$, and DIF_{SHPB} are the dynamic increase factor correspond to the quasi-static, drop weight impact, and SHPB tests, respectively. It is worth noting that these relationships are valid in the proposed range of strain rates. However, the experimental results obtained so far confirm these strain rate ranges. The transition strain rate ($\dot{\varepsilon}_{tr}$) is clearly dependent on the type of test and range of strain rate. The value of $1\,\text{s}^{-1}$ was proposed for transition strain rate ($\dot{\varepsilon}_{tr}$) between quasi-static and impact range correspond to drop weight test. While the value of $20\,\text{s}^{-1}$ was
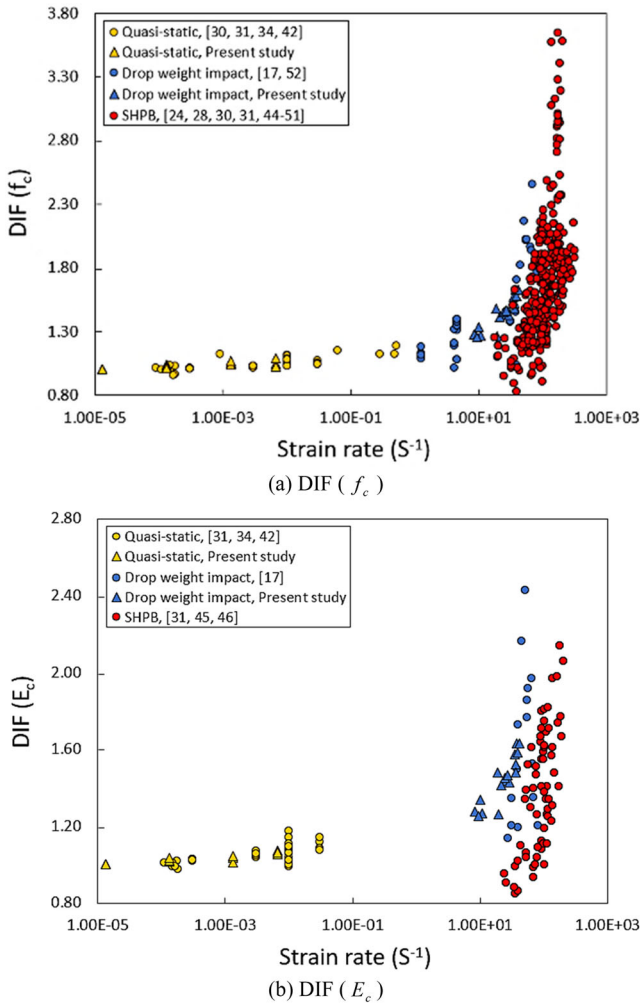
(a) DIF (f_c)

(b) DIF (E_c)

Figure 16. DIF for compressive strength of SFRC registered in the executed experimental program and in the literature.

Table 8. Coefficients in proposed DIF formula for SFRC.

Parameter	A	B	C	D	E	F
DIF (f_c)	12	1.67	1.16	0.20	−1.48	2.37
DIF (E_c)	10	0.96	1.26	0.50	−5.64	16.75
DIF (T)	12	2.74	1.05	6.88	−85.83	270.52

proposed for transition strain rate ($\dot{\varepsilon}_{tr}$) between quasi-static and impact range correspond to SHPB test, Table 8.

As shown in Figure 16, the values of modulus of elasticity for in the impact range using the drop weight impact test are greater than the SHPB test. Figure 17 shows the comparison of DIF (f_c) obtained from proposed models by other research and the present study with the experimental results. Evaluation of the proposed model in the present study was performed in the three different test approaches; quasi-static, drop weight impact, and SHPB. Figure 18 depicts the experimental DIF (E_c) obtained from three different test setups and their comparison with existing models and the proposed model in the present study. As shown in Figure 18, the proposed model can appropriately follow the trend of obtained DIF (E_c). While CEB-FIP model code [30] proposed a model for both range of quasi-static and impact. In the

current study, not only the effect of type of loading (quasi-static and impact) was considered, but also the effect of the test approach in the range of impact on the mechanical characteristics was evaluated.

To evaluate the accuracy of the models, mean absolute deviation (MAD) and mean absolute percentage error (MAPE) are used, according to Eqs. (11) and (12),

$$MAD = \left(\frac{1}{N}\right) \sum_1^N |pre_i - exp_i| \qquad (11)$$

$$MAPE = \left(\frac{1}{N}\right) \sum_1^N \left|\frac{pre_i - exp_i}{exp_i}\right| \times 100 \qquad (12)$$

where pre is the model prediction, exp is the experimental result, and N is the total number of specimens. The values of MAPE and MAD were calculated for each parameter and each test approach. Table 9 shows both MAPE and MAD values for the prediction of DIF (f_c) by different models. The results have shown that the model proposed by Hao and Hao [25] with MAPE and MAD of 8.65% and 0.09, respectively, has the biggest errors values in the range of quasi-static. While in the range of impact using drop weight test, two models proposed by Fujikake et al. [33] and Krahl et al. [37] predicted the experimental DIF (f_c) with the MAPE of 21.23% and 24.70% and MAD of 0.35 and 0.33, respectively. Regarding the results obtained from SHPB test, the model proposed by Fujikake et al. [33] show the highest MAPE and MAD of 6.91% and 0.09, respectively. While the prediction of the DIF (f_c) was improved by the proposed model with the lowest MAPE and MAD values, Table 9. It is realized that the proposed model in the present study predicts the DIF (f_c) more accurately considering the effect of both strain rate and test approach.

Two parameters of MAPE and MAD were also calculated for each test approach to evaluate the accuracy of the proposed models for the prediction of DIF (E_c), Table 10. Comparison of the obtained error values shows that the prediction of DIF (E_c) values is significantly improved by the proposed model. For instance, the values of MAD and MAPE that result from the model proposed by CEB-FIP model code [30] for the DIF (E_c) in the quasi-static range are 0.06 and 5.41%, respectively. While these values for the proposed model are 0.02 and 2.09%, respectively. Similarly, for impact tests using the drop weight impact and SHPB tests, the experimental DIF (E_c) can be predicted more accurately by the proposed model. While the model proposed by CEB-FIP model code [30] does not follow the trend of experimental results, especially for results obtained from the SHPB test. The proposed model in the present study can be used for the appropriate prediction of DIF (E_c).

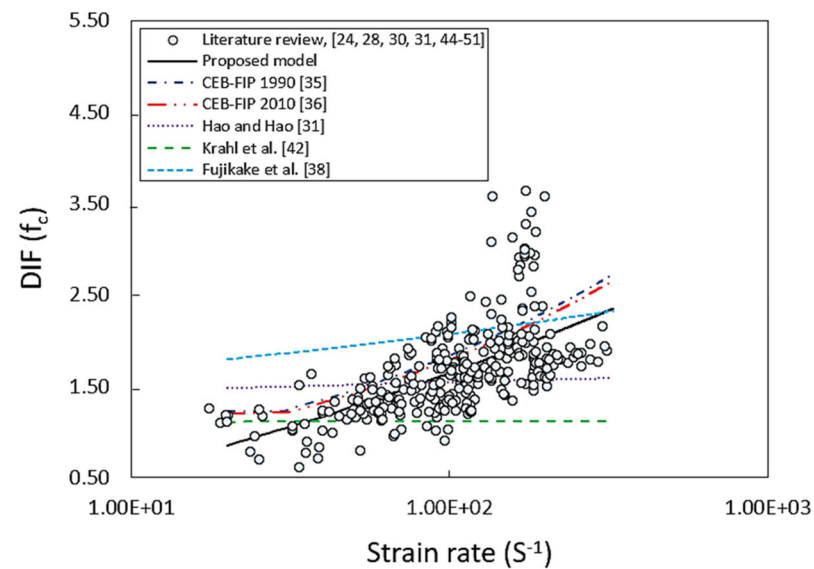### 3.5.2. Energy absorption capacity (toughness)

Toughness parameter is used to characterize the energy absorption capacity of SFRC in compression, and as larger it is, as ductile is the failure mode of SFRC structures failing in crushing [48]. Under quasi-static loading, it is considered
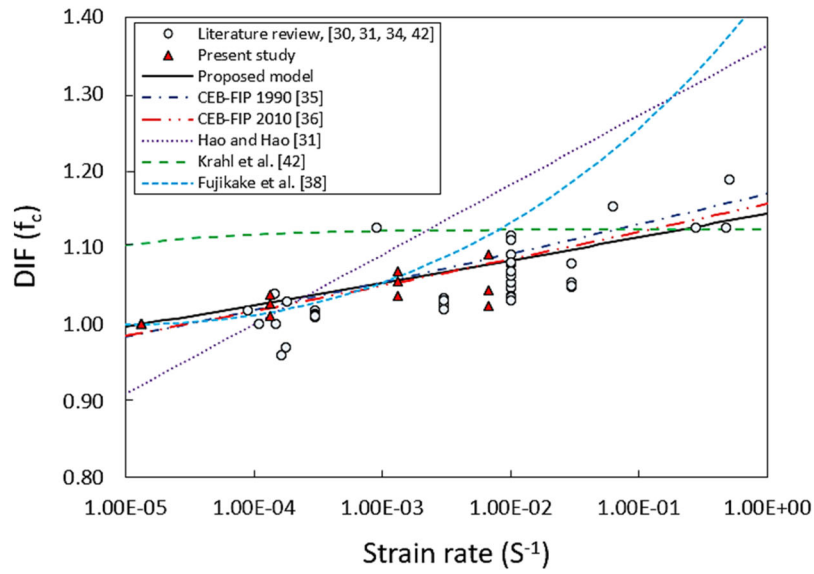
(a) DIF (f_c) – Quasi static
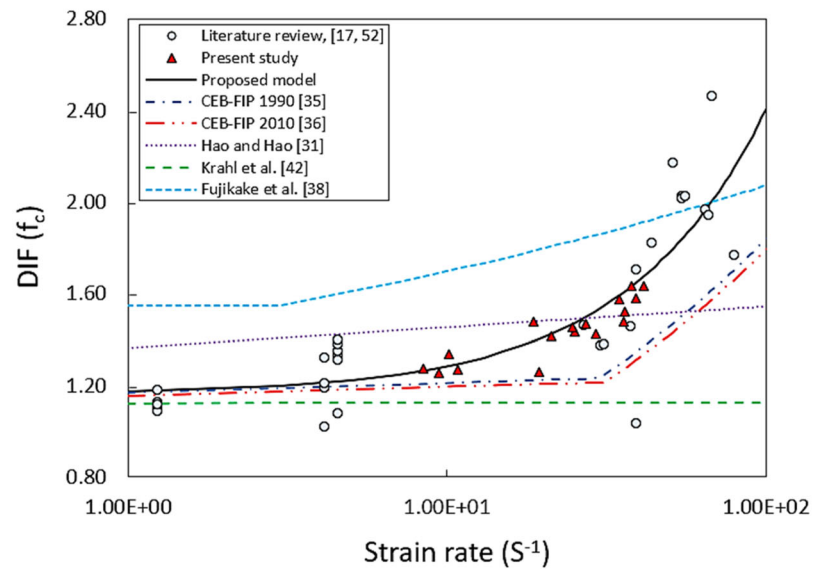
(b) DIF (f_c) – Drop weight impact

(c) DIF (f_c) – SHPB impact

Figure 17. Empirical DIF relations for SFRC's compressive strength using different test methods.
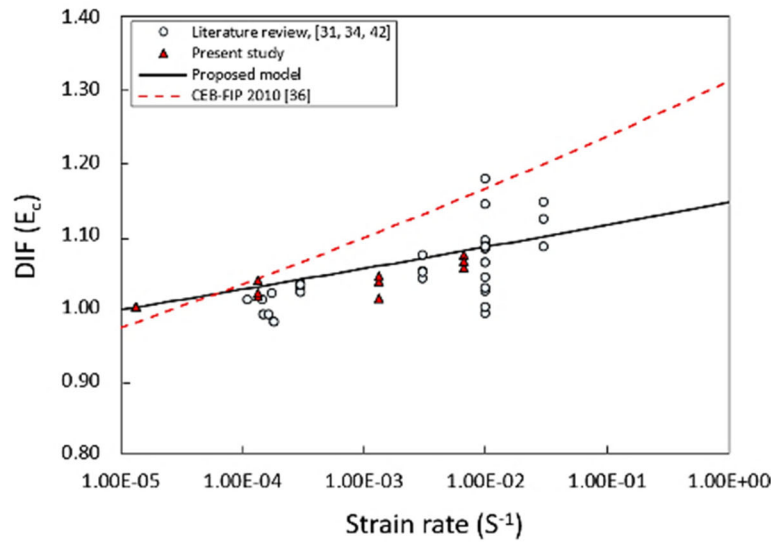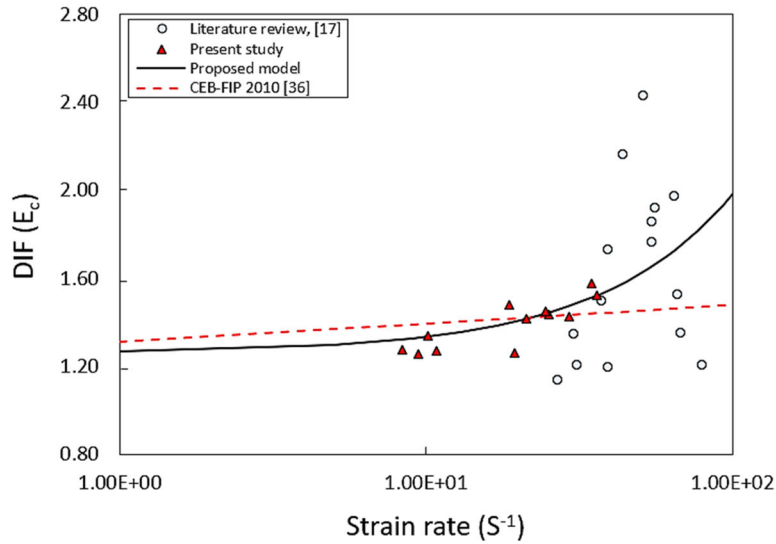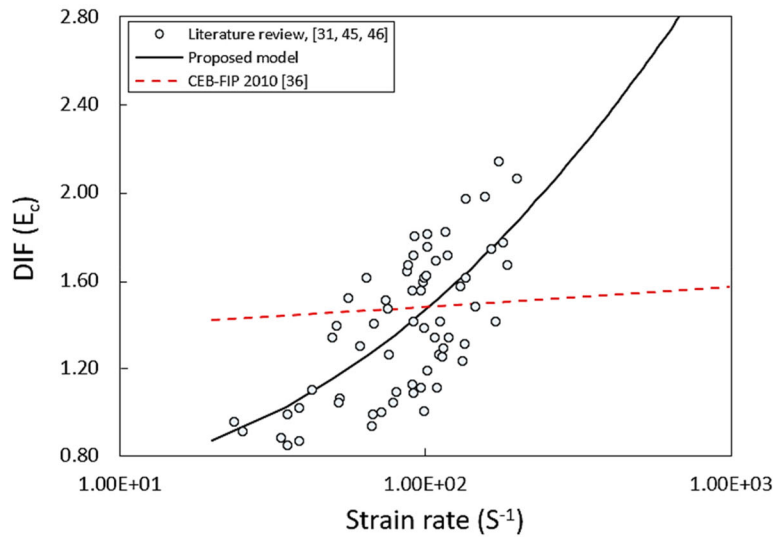
(a) DIF (E_c) – Quasi-static

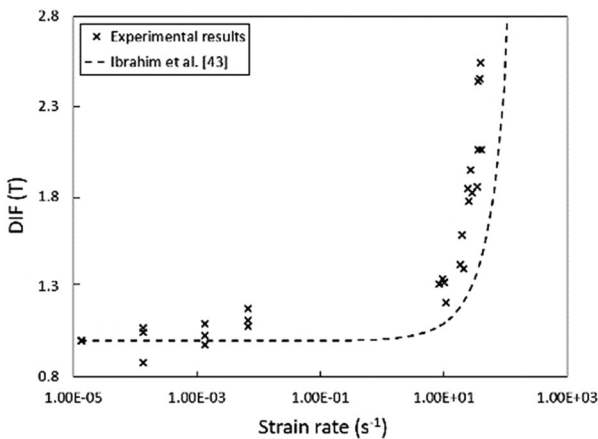(b) DIF (E_c) – Drop weight impact

(c) DIF (E_c) – SHPB impact

Figure 18. Empirical DIF relations for SFRC's modulus of elasticity using different test methods.

Table 9. MAPE and MAD values for prediction of DIF (f_c) by different models.

Reference	Quasi-static		Impact-drop weight		Impact-SHPB	
	MAPE	MAD	MAPE	MAD	MAPE	MAD
Proposed model	2.68	0.03	8.19	0.12	3.18	0.04
CEB-FIP [29]	3.02	0.03	13.37	0.21	4.17	0.06
CEB-FIP [30]	2.74	0.03	14.46	0.23	3.81	0.05
Hao and Hao [25]	8.65	0.09	13.80	0.20	2.56	0.04
Krahl et al. [37]	7.48	0.08	21.23	0.35	3.74	0.06
Fujikake et al. [33]	5.71	0.06	24.70	0.33	6.91	0.09

Table 10. MAPE and MAD values for prediction of DIF (E_c) by different models.

Reference	Quasi-static		Impact-drop weight		Impact-SHPB	
	MAPE	MAD	MAPE	MAD	MAPE	MAD
Proposed model	2.09	0.02	7.46	0.12	8.87	0.10
CEB-FIP [30]	5.41	0.06	8.19	0.14	16.37	0.17

Figure 20. Comparison of the obtained experimental DIF of toughness with the literature results.

Figure 19. (a) DIF of toughness of SFRC, (b) comparison of the obtained experimental DIF of toughness with the model proposed by Ibrahim et al. (38).

that the failure point in the compressive stress-strain curve corresponds to a strain value of 0.005.

Xu et al. [15] reported that due to a limitation in the displacement of hooked end fibers and the local damage that takes place near the hooks, the hooked end fiber has a relatively weaker mechanical bond to concrete than other steel fibers under impact loading. This limitation in the displacement of the fiber leads to a decrease in the ultimate strain of the SFRC and thus a lower toughness rather than other types of steel fibers is obtained (at the same strain rate in the range of impact). Consequently, the toughness under impact loading of SFRC with hooked end fibers mainly depends on the anchorage contribution of the fibers [49]. It should be noted that the efficiency of hooked end fibers in SFRC relies on the mechanical bond with concrete and the two end anchorages. The contribution of each in the energy dissipation can vary, depending on the strain rate considered [49]. Moreover, some experimental studies [24, 50] have investigated the effect of displacement rate in steel fiber pull-out test. They have shown that in the pull-out test, the rate sensitivity of the hooked end fibers is lower than the smooth fibers. Tarifa et al. [50] reported that this behavior of hooked end fiber is caused by the prevalence of the anchorage provided by the hook over the physicochemical bond. It makes the viscous-elastic/plastic response of the

concrete not completely develop, and consequently, the hooked end fibers have less sensitivity to the displacement rate. Considering previous research in this field that was discussed in the last paragraph, both the bond behavior and mechanical properties of hooked end fiber are the most important parameters influencing SFRC toughness, especially under impact loading. Likewise, the pull-out load and the mechanical properties of hooked end fibers are also determinant on the toughness of SFRC specimens subjected to different loading rates. In the present study, one type of hooked end fiber with specific mechanical properties was used for all the specimens.

The ratio of dynamic to static toughness for all SFRC specimens was listed in Table 6. The values presented show that the strain rate can significantly influence the toughness of SFRC. The maximum DIF for toughness presented in Table 6 is 2.54. Figure 19 shows the DIF values associated to toughness for the loading rates tested within the present research, and compares these with the results obtained with the model proposed by Ibrahim et al. [38]. This model underestimates the experimental results obtained in the present study. This can be attributed to the fact that this model has been derived from the experimental study performed by Ibrahim et al. [38] in which they used hybrid fibers (steel, polypropylene, and Kevlar fibers), and performed SHPB testing, while SFRC and the drop weight impact testing were the option in the current study. As shown in Figure 19, by increasing the strain rate, the difference between the results obtained from the model proposed by Ibrahim et al. [38] and the experimental results obtained in the present study is more visible.

The experimental results obtained in the current study and the results obtained in the experimental studies described by other research [15, 25, 28, 37, 38] on the DIF of toughness of SFRC specimens were plotted in Figure 20. As it is shown, the toughness value was more sensitive to the strain rate in the range of impact than in the range of quasi-static (Figure 21). Also, there are two main aspects to be noted when the current experimental results are compared with the previous studies. First, different toughness values are obtained at any strain rate. These differences increase with strain rate value and, in the impact range, are more obvious than in the quasi-static range. Second, the
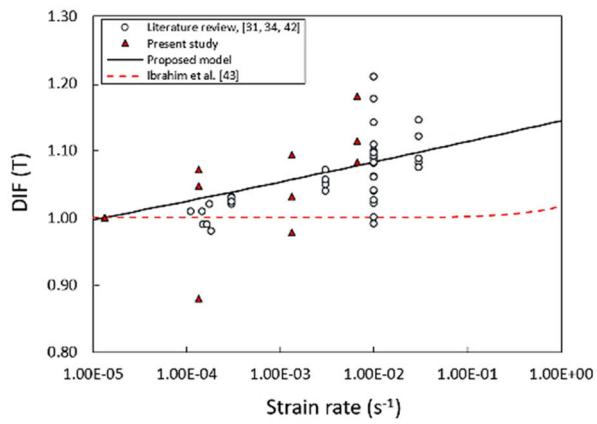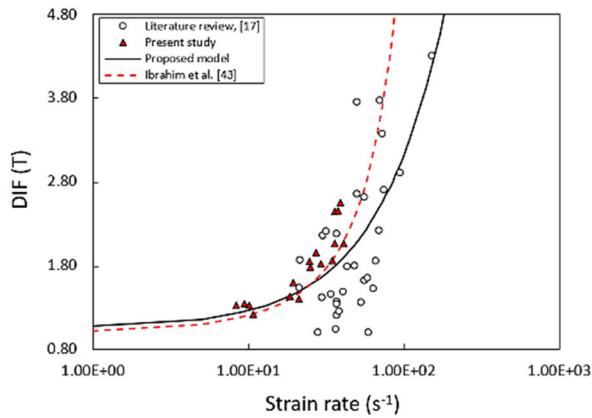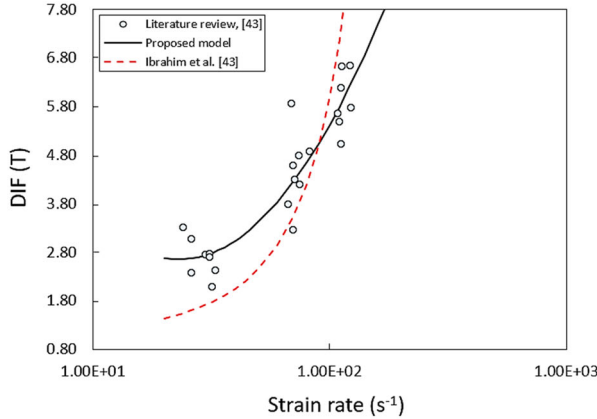
(a) DIF (T) – Quasi-static

(b) DIF (T) – Drop weight impact

(c) DIF (T) – SHPB impact

Figure 21. Empirical DIF relations for SFRC's toughness using different test methods.

Table 11. MAPE and MAD values for prediction of DIF (T) by different models.

Reference	Quasi-static		Impact-drop weight		Impact-SHPB	
	MAPE	MAD	MAPE	MAD	MAPE	MAD
Proposed model	2.95	0.03	21.82	0.35	10.58	0.43
Ibrahim et al. [38]	4.58	0.05	35.02	0.69	28.46	1.22

strain rates applied under impact loading are generally lower than the ones applied in the previous research, which means that the current work focuses on the lower strain rates range of impact. Considering these aspects, three empirical models were proposed to improve the prediction results of toughness considering the effect of both strain rate and test
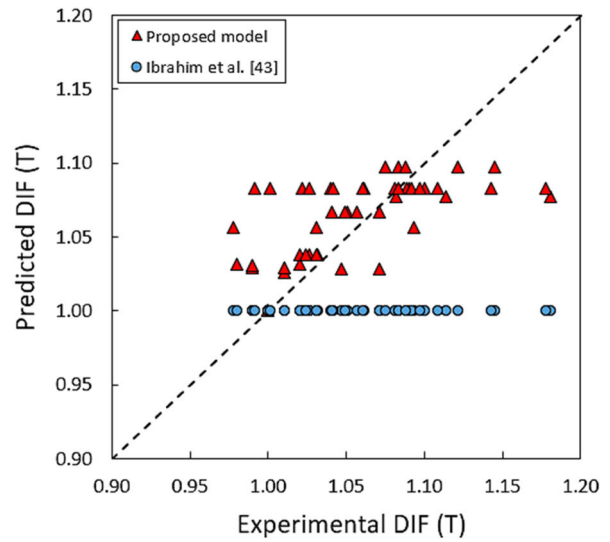
(a) DIF (T) – Quasi-static
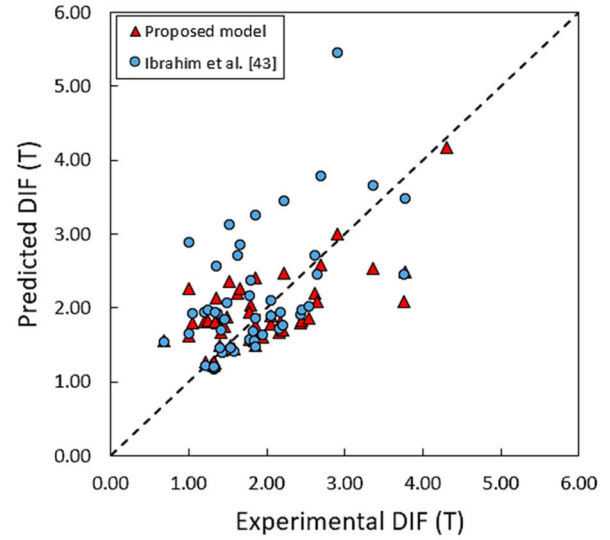
(b) DIF (T) – Drop weight impact
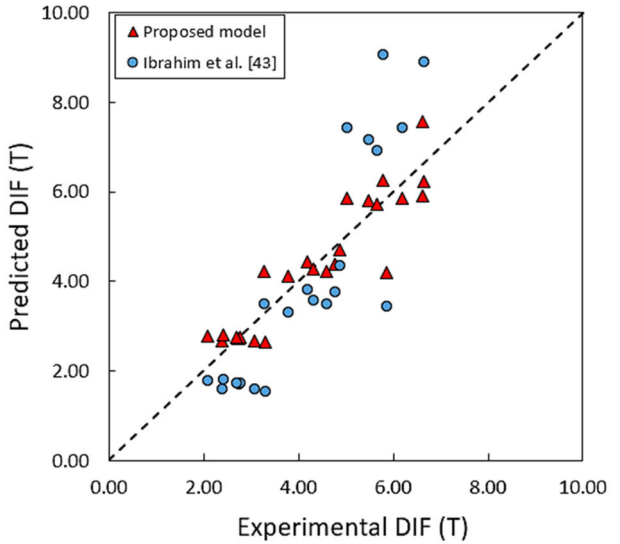
(c) DIF (T) – SHPB impact

Figure 22. Scatter in the prediction of DIF (T) using proposed models by Ibrahim et al. (38) and present study.

approach, Eqs. (9)–(11). Table 8 has shown the coefficient in proposed DIF formula for SFRC toughness.

MAPE and MAD values were calculated for each test approach to evaluation the accuracy of the proposed models for prediction of DIF (T), Table 11. Comparison of the obtained error values shows that the prediction of DIF (T) is improved by the proposed model. For instance, in the range of quasi-static, the model proposed by Ibrahim et al. [38] does not follow the trend of experimental results and the values of MAD and MAPE that result from the model proposed by Ibrahim et al. [38] for the DIF (T) in the quasi-static range are 0.05 and 4.58%, respectively. While these values for the proposed model are 0.02 and 2.09%, respectively. Similarly, for impact tests using the drop weight impact and SHPB tests, the experimental DIF (T) can be predicted more accurately by the proposed model, Table 11.

The scatter in the prediction of DIF (T) using proposed models by Ibrahim et al. [38] and present study was shown in Figure 22. The proposed empirical formula can be used to estimate the DIF in the numerical and analytical prediction of SFRC structure responses under high strain rate loadings. It should be noted that proposed models are derived from test data for the strain rates up to $313.4\,s^{-1}$ for three different test approaches. Beyond this range and the use of another testing approach, the proposed model can be modified for them.

4. Conclusions

The current study investigated the effect of strain rate on the compressive behavior of steel fiber reinforced concrete (SFRC) in both range of the quasi-static and impact. For this purpose, an experimental study was performed on 29 SFRC cylinders under compressive loading. Compressive strength, modulus of elasticity and toughness were evaluated under eight different strain rates, ranging from quasi-static (between 10^{-6} and $10^{-2}\ s^{-1}$) to impact level (between 1 and $50\,s^{-1}$). The paper also investigated the inertia force effects during compressive impact process and its relationship with the acceleration. The study on the strain rate effect is based on the dynamic increase factor (DIF), and this parameter was analyzed and calculated for compressive strength, modulus of elasticity and toughness. In addition, the calculated DIFs based on the experimental results were compared with DIF proposed models by present study, by CEB-FIP codes and by other researchers. This comparison was aimed at evaluating the applicability of the different models in predicting the effect of high strain rates on the above-mentioned SFRC characteristics. Based on the results and observations of this study, the following conclusions were reached:

1. The maximum acceleration at the mid height of the cylinder and subsequently the inertia force increase as the strain rate increases. The difference between experimental and analytical inertia forces also increases with strain rate. Also, a non-linear acceleration distribution along the specimen is expected, and the assumption of linear distribution is not applicable for all ranges of strain rate studied.

2. By increasing the strain rate, modulus of elasticity, compressive strength, and toughness of SFRC increase. The strain rate effect in the range of impact is more significant than in the range of quasi-static loading.

3. Corresponds to the maximum strain rate obtained, maximum DIF values of 1.58, 1.48, and 2.54 were achieved for the modulus of elasticity, compressive strength, and toughness, respectively. The maximum DIF values of these parameters show that the strain rate can significantly influence the mechanical properties of SFRC.

4. In addition to the strain rate, the effect of test approach was considered by proposed models. Three different models were established for predicting each mechanical characteristic of SFRC at the different strain rates; one model in the range of quasi-static and two models in the range of impact correspond to the SHPB and drop weight impact tests.

5. The DIF models of modulus of elasticity, compressive strength, and toughness proposed by present study can predict DIF values of SFRC more accurately than the other models considered.

Author contributions

Disclosure statement

Funding

References

[1] N. Banthia, C. Yan, and K. Sakai, Impact resistance of fiber reinforced concrete at subnorma temperatures, Cem. Concr. Compos., vol. 20, no. 5, pp. 393–404, 1998. DOI: 10.1016/S0958-9465(98)00015-8.

[2] ACI Committee 544, Measurement of Properties of Fibre Reinforced Concrete, 1989.

[3] V.M.C.F. Cunha, J.A.O. Barros, and J.M. Sena-Cruz, Pullout behavior of steel fibers in self-compacting concrete, J. Mater. Civ. Eng., vol. 22, no. 1, pp. 1–9, 2010. DOI: 10.1061/(ASCE)MT.1943-5533.0000001.

[4] S. Naderi and M. Zhang, 3D meso-scale modelling of tensile and compressive fracture behaviour of steel fibre reinforced

concrete, Compos. Struct., vol. 291, pp. 115690, 2022. DOI: 10.1016/j.compstruct.2022.115690.

[5] G. Murali, J. Venkatesh, N. Lokesh, T.R. Nava, and K. Karthikeyan, Comparative experimental and analytical modeling of impact energy dissipation of ultra-high performance fibre reinforced concrete, KSCE J. Civ. Eng., vol. 22, no. 8, pp. 3112–3119, 2018. DOI: 10.1007/s12205-017-1678-3.

[6] ACI Committee 544, State-of-the-Art Report on Fiber Reinforced Concrete, 1996.

[7] D.-Y. Yoo, S.-T. Kang, and Y.-S. Yoon, Enhancing the flexural performance of ultra-high-performance concrete using long steel fibers, Compos. Struct., vol. 147, pp. 220–230, 2016. DOI: 10.1016/j.compstruct.2016.03.032.

[8] F. Soltanzadeh, V.M.C.F. Cunha, and J.A.O. Barros, Assessment of different methods for characterization and simulation of post-cracking behavior of self-compacting steel fiber reinforced concrete, Constr. Build. Mater., vol. 227, p. 116704, 2019. DOI: 10.1016/j.conbuildmat.2019.116704.

[9] H. Salehian and J.A.O. Barros, Assessment of the performance of steel fibre reinforced self-compacting concrete in elevated slabs, Cem. Concr. Compos., vol. 55, pp. 268–280, 2015. DOI: 10.1016/j.cemconcomp.2014.09.016.

[10] X. Lu, Y. Zhang, H. Zhang, H. Zhang, and R. Xiao, Experimental study on seismic performance of steel fiber reinforced high strength concrete composite shear walls with different steel fiber volume fractions, Eng. Struct., vol. 171, pp. 247–259, 2018. DOI: 10.1016/j.engstruct.2018.05.068.

[11] N. Banthia and S. Mindess, Impact resistance of steel fiber reinforced concrete, Mater. J., vol. 93, pp. 472–479, 1996.

[12] X.X. Zhang, A.M. Abd Elazim, G. Ruiz, and R.C. Yu, Fracture behaviour of steel fibre-reinforced concrete at a wide range of loading rates, Int. J. Impact Eng., vol. 71, pp. 89–96, 2014. DOI: 10.1016/j.ijimpeng.2014.04.009.

[13] X. Dong and J. Gao. Effects of fiber type and fiber volume content on frost resistance of fiber-reinforced concrete in airport pavement, In: ICTE 2011, pp. 1524–1529, 2011. DOI: 10.1061/41184(419)252.

[14] H. Ye, Z. Yang, and B. Han, Failure mechanisms governing fatigue strength of steel–SFRC composite bridge deck with U-ribs, J. Bridge Eng., vol. 26, p. 4021014, 2021.

[15] Z. Xu, H. Hao, and H.N. Li, Experimental study of dynamic compressive properties of fibre reinforced concrete material with different fibres, Mater. Des., vol. 33, pp. 42–55, 2012. DOI: 10.1016/j.matdes.2011.07.004.

[16] D.-Y. Yoo, and N. Banthia, Impact resistance of fiber-reinforced concrete—A review, Cem. Concr. Compos., vol. 104, p. 103389, 2019. DOI: 10.1016/j.cemconcomp.2019.103389.

[17] P.H. Bischoff and S.H. Perry, Compressive behaviour of concrete at high strain rates, Mater. Struct., vol. 24, no. 6, pp. 425–450, 1991. DOI: 10.1007/BF02472016.

[18] T.S. Lok, P.J. Zhao, and G. Lu, Using the split Hopkinson pressure bar to investigate the dynamic behaviour of SFRC, Mag. Concr. Res., vol. 55, no. 2, pp. 183–191, 2003. DOI: 10.1680/macr.2003.55.2.183.

[19] T.S. Lok and P.J. Zhao, Impact response of steel fiber-reinforced concrete using a split Hopkinson pressure bar, J. Mater. Civ. Eng., vol. 16, no. 1, pp. 54–59, 2004. DOI: 10.1061/(ASCE)0899-1561(2004)16:1(54).

[20] S. Wang, M.-H. Zhang, and S.T. Quek, Effect of specimen size on static strength and dynamic increase factor of high-strength concrete from SHPB test, J. Test. Eval., vol. 39, no. 5, pp. 898–907, 2011. DOI: 10.1520/JTE103370.

[21] S. Wang, M.-H. Zhang, and S.T. Quek, Effect of high strain rate loading on compressive behaviour of fibre-reinforced high-strength concrete, Mag. Concr. Res., vol. 63, no. 11, pp. 813–827, 2011. DOI: 10.1680/macr.2011.63.11.813.

[22] A.S. Savinykh, G.V. Garkushin, G.I. Kanel, and S.V. Razorenov, Compressive and tensile strength of steel fibrous reinforced concrete under explosive loading, Int. J. Fract., vol. 215, no. 1–2, pp. 129–138, 2019. DOI: 10.1007/s10704-018-00342-w.

[23] Y.K. Hwang, J.E. Bolander, and Y.M. Lim, Evaluation of dynamic tensile strength of concrete using lattice-based simulations of spalling tests, Int. J. Fract., vol. 221, no. 2, pp. 191–209, 2020. DOI: 10.1007/s10704-020-00422-w.

[24] E. Poveda, R.C. Yu, M. Tarifa, G. Ruiz, V.M. Cunha, and J.A. Barros, Rate effect in inclined fibre pull-out for smooth and hooked-end fibres: A numerical study, Int. J. Fract., vol. 223, no. 1–2, pp. 135–149, 2020. DOI: 10.1007/s10704-019-00404-7.

[25] Y. Hao and H. Hao, Dynamic compressive behaviour of spiral steel fibre reinforced concrete in split Hopkinson pressure bar tests, Constr. Build. Mater., vol. 48, pp. 521–532, 2013. DOI: 10.1016/j.conbuildmat.2013.07.022.

[26] L. Yang, X. Lin, and R.J. Gravina, Evaluation of dynamic increase factor models for steel fibre reinforced concrete, Constr. Build. Mater., vol. 190, pp. 632–644, 2018. DOI: 10.1016/j.conbuildmat.2018.09.085.

[27] L. Yang, X. Lin, H. Li, and R.J. Gravina, A new constitutive model for steel fibre reinforced concrete subjected to dynamic loads, Compos. Struct., vol. 221, p. 110849, 2019. DOI: 10.1016/j.compstruct.2019.04.021.

[28] H. Othman, H. Marzouk, and M. Sherif, Effects of variations in compressive strength and fibre content on dynamic properties of ultra-high performance fibre-reinforced concrete, Constr. Build. Mater., vol. 195, pp. 547–556, 2019. DOI: 10.1016/j.conbuildmat.2018.11.093.

[29] CEB-FIP, Design code 1990, Com Euro Int du Bet., pp. 51–59, 1990.

[30] CEB-FIP, Model code 2010, Com Euro-International du Bet., 2010.

[31] ACI Committee 544, Report on Measuring Mechanical Properties of Hardened Fiber Reinforced Concrete, 2017.

[32] L.J. Malvar, Review of static and dynamic properties of steel reinforcing bars, Mater. J., vol. 95, pp. 609–616, 1998.

[33] K. Fujikake, K. Mori, K. Uebayashi, T. Ohno, and J. Mizuno, Constitutive model for concrete materials with high-rates of loading under tri-axial compressive stress states, In: Proc., 3rd Int. Conf. on Concrete under Severe Conditions, JSCE, Tokyo, pp. 636–643, 2001.

[34] S. Mindess and L. Zhang, Impact resistance of fibre-reinforced concrete, Proc. Inst. Civ. Eng. Build., vol. 162, no. 1, pp. 69–76, 2009. DOI: 10.1680/stbu.2009.162.1.69.

[35] O. Hjorth, A Contribution to the Problem of Strength and Bond Relationships for Steel and Concrete at High Loading Rates, Universitat Carolo-Wilhelmina, Braunschweig, 1976.

[36] R.R. Craig Jr and A.J. Kurdila, Fundamentals of Structural Dynamics, John Wiley & Sons, Hoboken, New Jersey. 2006.

[37] P.A. Krahl, G.M.S. de Gidrão, and R. Carrazedo, Compressive behavior of UHPFRC under quasi-static and seismic strain rates considering the effect of fiber content, Constr. Build. Mater., vol. 188, pp. 633–644, 2018. DOI: 10.1016/j.conbuildmat.2018.08.121.

[38] S.M. Ibrahim, T.H. Almusallam, Y.A. Al-Salloum, A.A. Abadel, and H. Abbas, Strain rate dependent behavior and modeling for compression response of hybrid fiber reinforced concrete, Lat. Am. J. Solids Struct., vol. 13, no. 9, pp. 1695–1715, 2016. DOI: 10.1590/1679-78252717.

[39] S.H. Yan, Q.H. Qian, and X.Q. Jiang, Comparative test and analysis on static and dynamic compressive characteristics of short steel fiber reinforced concrete, China Concr. Cem. Prod., vol. 1, pp. 33–35, 2001.

[40] M.H. Zhang, M.S.H. Sharif, and G. Lu, Impact resistance of high-strength fibre-reinforced concrete, Mag Concr Res., vol. 59, no. 3, pp. 199–210, 2007. DOI: 10.1680/macr.2007.59.3.199.

[41] J. Lai and W. Sun, Dynamic mechanical behaviour of ultra-high performance fiber reinforced concretes, J. Wuhan Univ. Technol. Mater. Sci. Ed., vol. 23, no. 6, pp. 938–945, 2008. DOI: 10.1007/s11595-007-6938-5.

[42] Y. Ju, H. Liu, G. Sheng, and H. Wang, Experimental study of dynamic mechanical properties of reactive powder concrete

under high-strain-rate impacts, Sci. China Technol. Sci., vol. 53, no. 9, pp. 2435–2449, 2010. DOI: 10.1007/s11431-010-4061-x.

[43] Z. Rong, W. Sun, and Y. Zhang, Dynamic compression behavior of ultra-high performance cement based composites, Int J Impact Eng., vol. 37, no. 5, pp. 515–520, 2010. DOI: 10.1016/j.ijimpeng.2009.11.005.

[44] S. Wang, M.-H. Zhang, and S.T. Quek, Mechanical behavior of fiber-reinforced high-strength concrete subjected to high strain-rate compressive loading, Constr. Build. Mater., vol. 31, pp. 1–11, 2012. DOI: 10.1016/j.conbuildmat.2011.12.083.

[45] Y. Su, J. Li, C. Wu, P. Wu, and Z.X. Li, Effects of steel fibres on dynamic strength of UHPC, Constr. Build. Mater., vol. 114, pp. 708–718, 2016. DOI: 10.1016/j.conbuildmat.2016.04.007.

[46] A.B. Groeneveld, T.M. Ahlborn, C.K. Crane, and W.R. Long, Effect of Fiber Orientation on Dynamic Compressive Properties of an Ultra-High Performance Concrete, US Army Engineer Research and Development Center, Vicksburg, MS, 2017.

[47] G.M. Ren, H. Wu, Q. Fang, and J.Z. Liu, Effects of steel fiber content and type on dynamic compressive mechanical properties of UHPCC, Constr. Build. Mater., vol. 164, pp. 29–43, 2018. DOI: 10.1016/j.conbuildmat.2017.12.203.

[48] A. Edalat-Behbahani, J.A.O. Barros, and A. Ventura-Gouveia, Application of plastic-damage multidirectional fixed smeared crack model in analysis of RC structures, Eng. Struct., vol. 125, pp. 374–391, 2016. DOI: 10.1016/j.engstruct.2016.07.013.

[49] N. Banthia and J.-F. Trottier, Deformed steel fiber—Cementitious matrix bond under impact, Cem. Concr. Res., vol. 21, no. 1, pp. 158–168, 1991. DOI: 10.1016/0008-8846(91)90042-G.

[50] M. Tarifa, E. Poveda, V.M.C.F. Cunha, and J.A.O. Barros, Effect of the displacement rate and inclination angle in steel fiber pullout tests, Int. J. Fract., vol. 223, no. 1–2, pp. 109–122, 2020. DOI: 10.1007/s10704-019-00398-2.